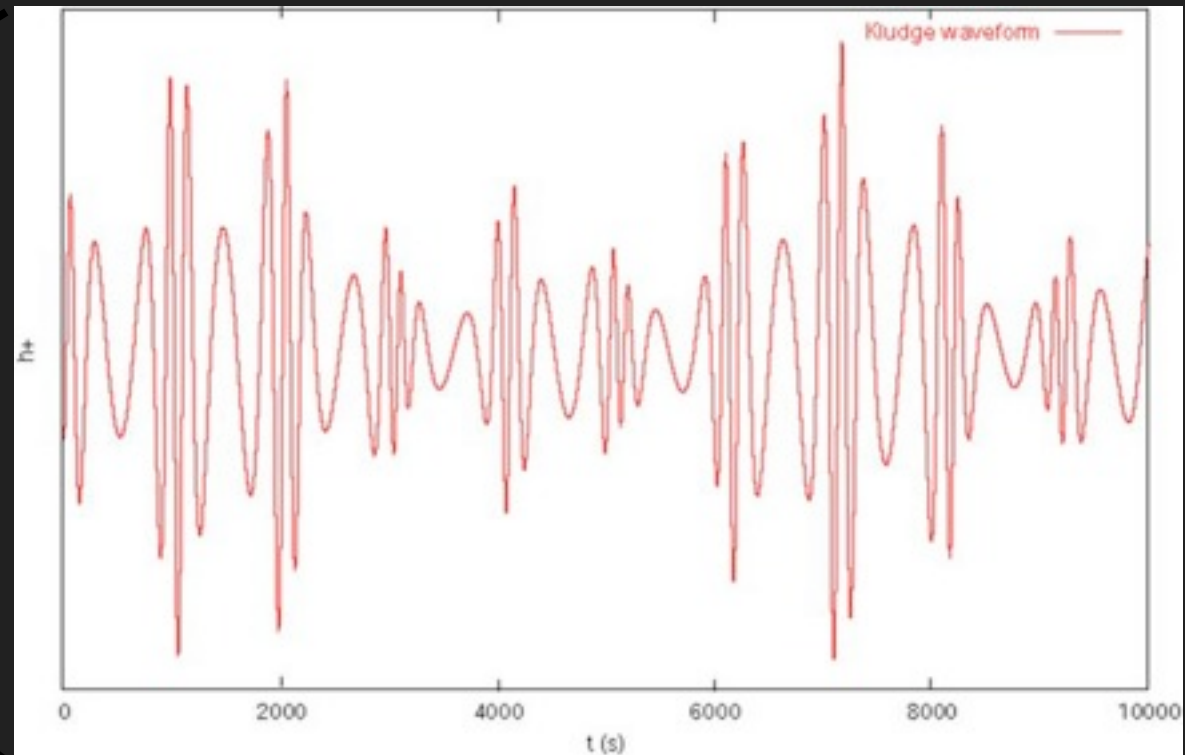


“Kludge” techniques and self-forced evolution

Jonathan Gair, Institute of Astronomy, Cambridge, UK
Capra Meeting, Southampton, July 7th 2011



Talk Outline

- The need for approximate waveform models
- “Numerical kludge” approach to waveform modelling
 - Description of method
 - Computation of corresponding gravitational waveforms
 - Tests and applications of the kludge models
- Self-forced evolution
 - Method of osculating elements
 - Application to EMRI evolution under perturbing forces
 - Gravitational self-forced evolution in Schwarzschild
- Collaborators: Stanislav Babak, Rob Cole, Steve Drasco, Eanna Flanagan, Kostas Glampedakis, Tanja Hinderer, Scott Hughes and Eliu Huerta.

Kludge Techniques

JG & K. Glampedakis, PRD 73 064037 (2006)

S. Babak, H. Fang, JG, K. Glampedakis & S. Hughes, PRD 75 024005 (2007)

The need for approximate waveforms

- Computation of template space metrics requires evaluation of waveform derivatives – must compute many nearby waveforms and iterate at each point in parameter space.
- Need techniques to compute realistic waveforms quickly and cheaply – develop “kludge” approaches that capture the main features of generic EMR inspirals but are quicker and cheaper to generate than full self-forced evolutions.
- “Kludge”:
 - ‘A system, especially a computer system, that is constructed of poorly matched elements or of elements originally intended for other applications’ (American Heritage Dictionary).
 - ‘A clumsy or inelegant solution to a problem’ (American Heritage Dictionary).
 - ‘Something hastily or badly put together’ (AskOxford.com).

“Analytic kludge” (Barack & Cutler 2004)

- Use Keplerian (Peters and Mathews) waveforms as a basis.
- Add relativistic effects using post-Newtonian results
 - Perihelion precession and precession of orbital plane.
 - Evolution of orbital parameters (frequency, eccentricity) over the inspiral.
- Include low-frequency approximation to the LISA detector response.
- Analytic kludge waveforms can be computed very quickly, but are hard to match onto perturbative computations, as the parameterisation is different

“Numerical kludge”

- Compute a phase space trajectory by integrating a prescription for \dot{E} , \dot{L}_z and \dot{Q} as functions of E , L_z and Q (adiabatic approximation).
- Integrate the Kerr geodesic equations numerically for resultant $E(t)$, $L_z(t)$ and $Q(t)$ to give $r(t)$, $\theta(t)$ and $\phi(t)$

$$\Sigma^2 \left(\frac{dr}{d\tau} \right)^2 = \left[(r^2 + a^2) E - aL_z \right]^2 - \Delta \left[r^2 + (L_z - aE)^2 + Q \right]$$

$$\Sigma^2 \left(\frac{d\theta}{d\tau} \right)^2 = Q - \cot^2 \theta L_z^2 - a^2 \cos^2 \theta (1 - E^2)$$

$$\Sigma \left(\frac{d\phi}{d\tau} \right) = \csc^2 \theta L_z + aE \left(\frac{r^2 + a^2}{\Delta} - 1 \right) - \frac{a^2 L_z}{\Delta}$$

$$\Sigma \left(\frac{dt}{d\tau} \right) = E \left[\frac{(r^2 + a^2)^2}{\Delta} - a^2 \sin^2 \theta \right] + aL_z \left(1 - \frac{r^2 + a^2}{\Delta} \right)$$

“Numerical kludge”

- Identify Boyer-Lindquist coordinates (r, θ, φ) with flat space spherical polar coordinates. Construct approximate gravitational waveform from resulting flat space quadrupole moment tensor (“particle on a string”).
- Include detector modulations using low-frequency approximation to LISA response.
- Numerical kludge waveforms are more computationally intensive to generate than the analytic ones but
 - They may be easily identified with perturbative waveforms since they are based on a Kerr geodesic parameterisation.
 - The fundamental frequencies are instantaneously correct, again due to the Kerr geodesic basis.
 - It is easy to incorporate additional physical effects into the model.

Geodesic parameterization

- Instead of E , L_z and Q , introduce a semi-latus rectum, eccentricity and orbital inclination angle (p, e, ι) .
- Find the extrema of the orbit, r_p, r_a , which are roots of the radial geodesic equation

$$R(r) = \left[(r^2 + a^2) E - aL_z \right]^2 - \Delta \left[r^2 + (L_z - aE)^2 + Q \right]$$

- Define p and e using the Keplerian definitions

$$r_p = \frac{p}{1+e}, \quad r_a = \frac{p}{1-e} \quad \Rightarrow \quad e = \frac{r_a - r_p}{r_a + r_p}, \quad p = \frac{2r_a r_p}{r_a + r_p}$$

- Define an inclination angle, ι , in terms of L_z and Q by

$$Q = L_z^2 \tan^2 \iota$$

Phase-space trajectories

- Basic idea (Glampedakis, Hughes & Kennefick 2002) – use post-Newtonian energy and angular momentum fluxes.

$$\frac{dE}{dt} = -\frac{32}{5} \frac{\mu^2}{M^2} \left(\frac{M}{p}\right)^5 (1-e^2)^{3/2} \left[f_1(e) - \frac{a}{M} \left(\frac{M}{p}\right)^{3/2} \cos \iota f_2(e) \right],$$

$$\frac{dL_z}{dt} = -\frac{32}{5} \frac{\mu^2}{M} \left(\frac{M}{p}\right)^{7/2} (1-e^2)^{3/2} \left[\cos \iota f_3(e) + \frac{a}{M} \left(\frac{M}{p}\right)^{3/2} [f_4(e) - \cos^2 \iota f_5(e)] \right]$$

$$f_1(e) = 1 + \frac{73}{24}e^2 + \frac{37}{96}e^4, \quad f_2(e) = \frac{73}{12} + \frac{823}{24}e^2 + \frac{949}{32}e^4 + \frac{491}{192}e^6, \quad f_3(e) = 1 + \frac{7}{8}e^2,$$

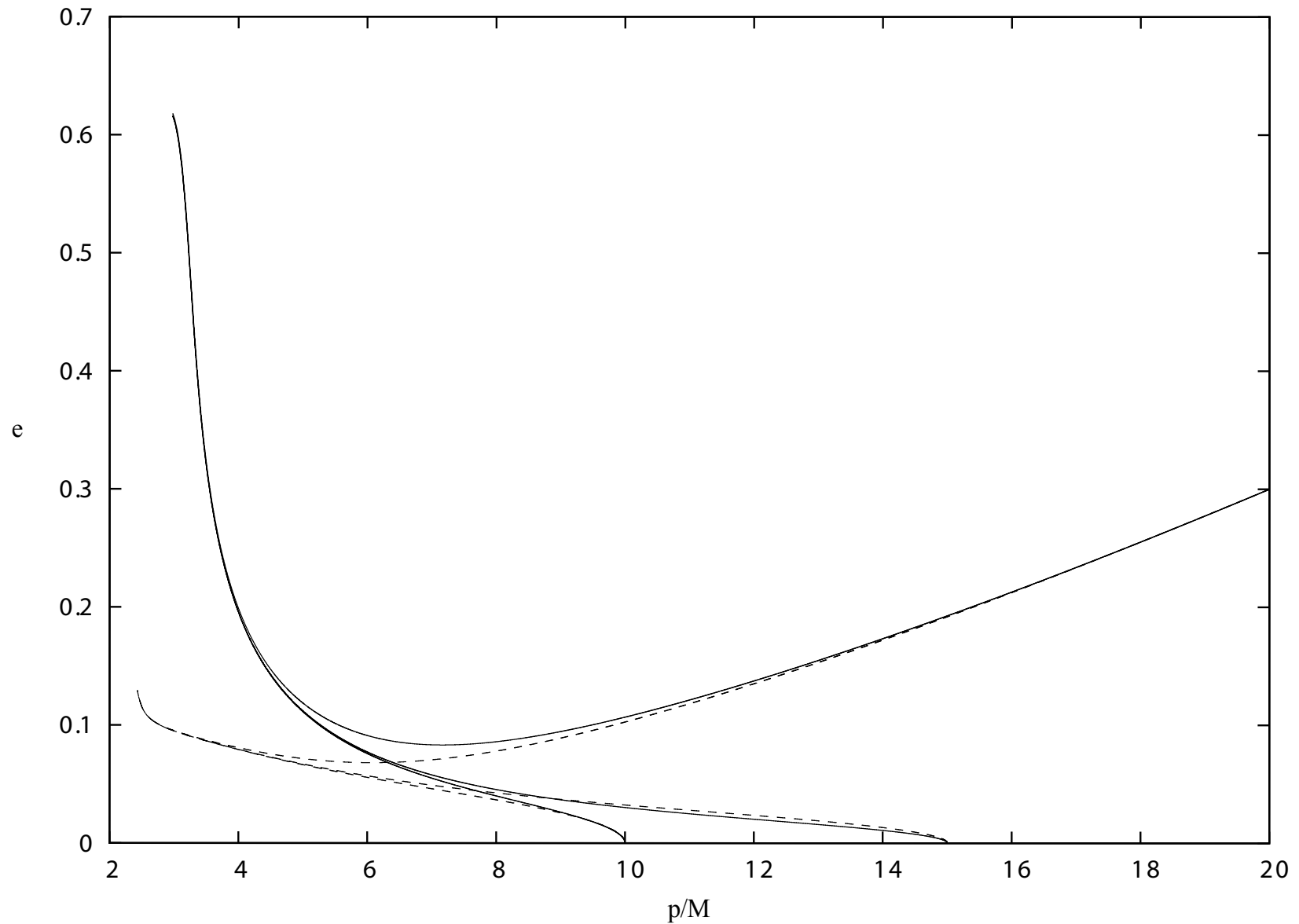
$$f_4(e) = \frac{61}{24} + \frac{63}{8}e^2 + \frac{95}{64}e^4, \quad f_5(e) = \frac{61}{8} + \frac{91}{4}e^2 + \frac{461}{64}e^4, \quad f_6(e) = \frac{97}{12} + \frac{37}{2}e^2 + \frac{211}{32}e^4$$

- GHK also took $i = 0$, to avoid overpredicting inclination change.
- This approach exhibited some pathological behaviour.

Consistency corrections

- GHK inspirals showed pathological behaviour for near-circular orbits, $de/dt \propto 1/e$.

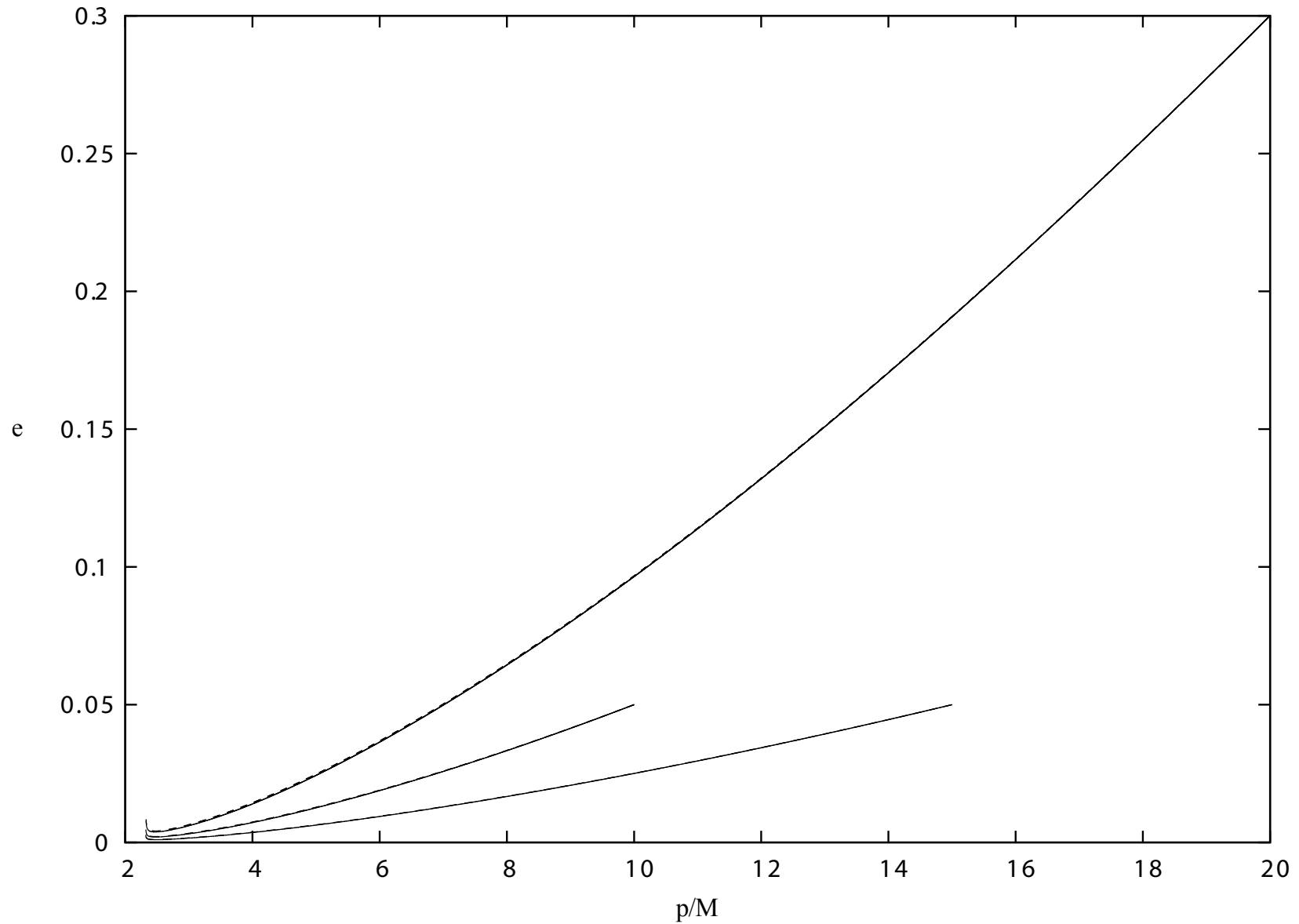
Consistency corrections



Consistency corrections

- GHK inspirals showed pathological behaviour for near-circular orbits, $de/dt \propto 1/e$.
- This arose from transforming between (E, L_z, Q) and (e, p, ι) - necessary cancellations occur only at PN order of the fluxes.
- Correct by forcing circular orbits to remain circular - use PN expression for \dot{E}, \dot{Q} to determine circular part of \dot{L}_z .

Consistency corrections

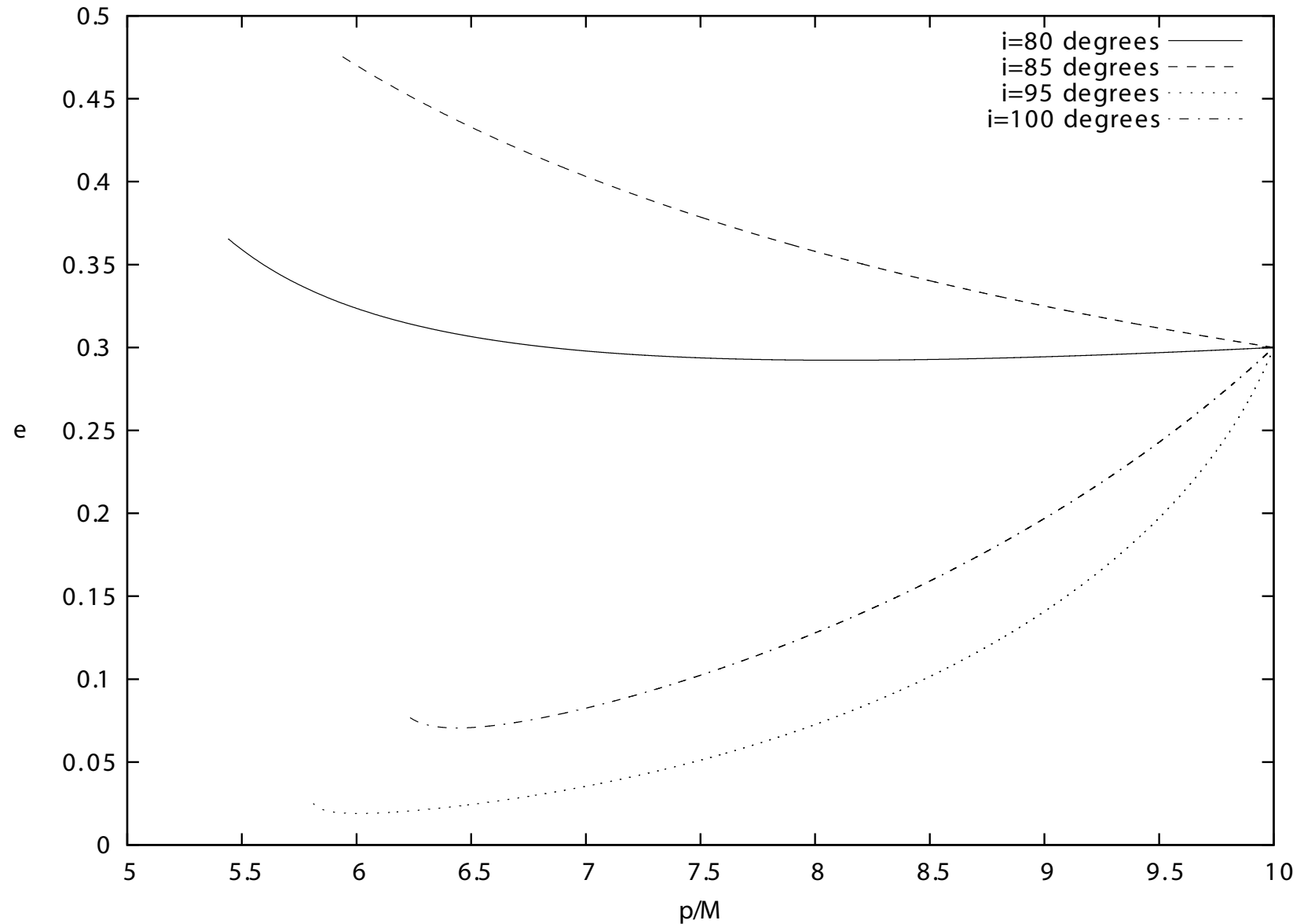


Consistency corrections

- GHK inspirals showed pathological behaviour for near-circular orbits, $de/dt \propto 1/e$.
- This arose from transforming between (E, L_z, Q) and (e, p, ι) - necessary cancellations occur only at PN order of the fluxes.
- Correct by forcing circular orbits to remain circular - use PN expression for \dot{E}, \dot{Q} to determine circular part of \dot{L}_z .
- Constant inclination assumption also gives rise to pathological behaviour for polar orbits since

$$\frac{dQ}{dt} = 2 \sqrt{Q} \frac{\sin \iota}{\cos \iota} \left(\frac{dL_z}{dt} + \sqrt{Q} \frac{1}{\sin^2 \iota} \frac{d\iota}{dt} \right)$$

Consistency corrections



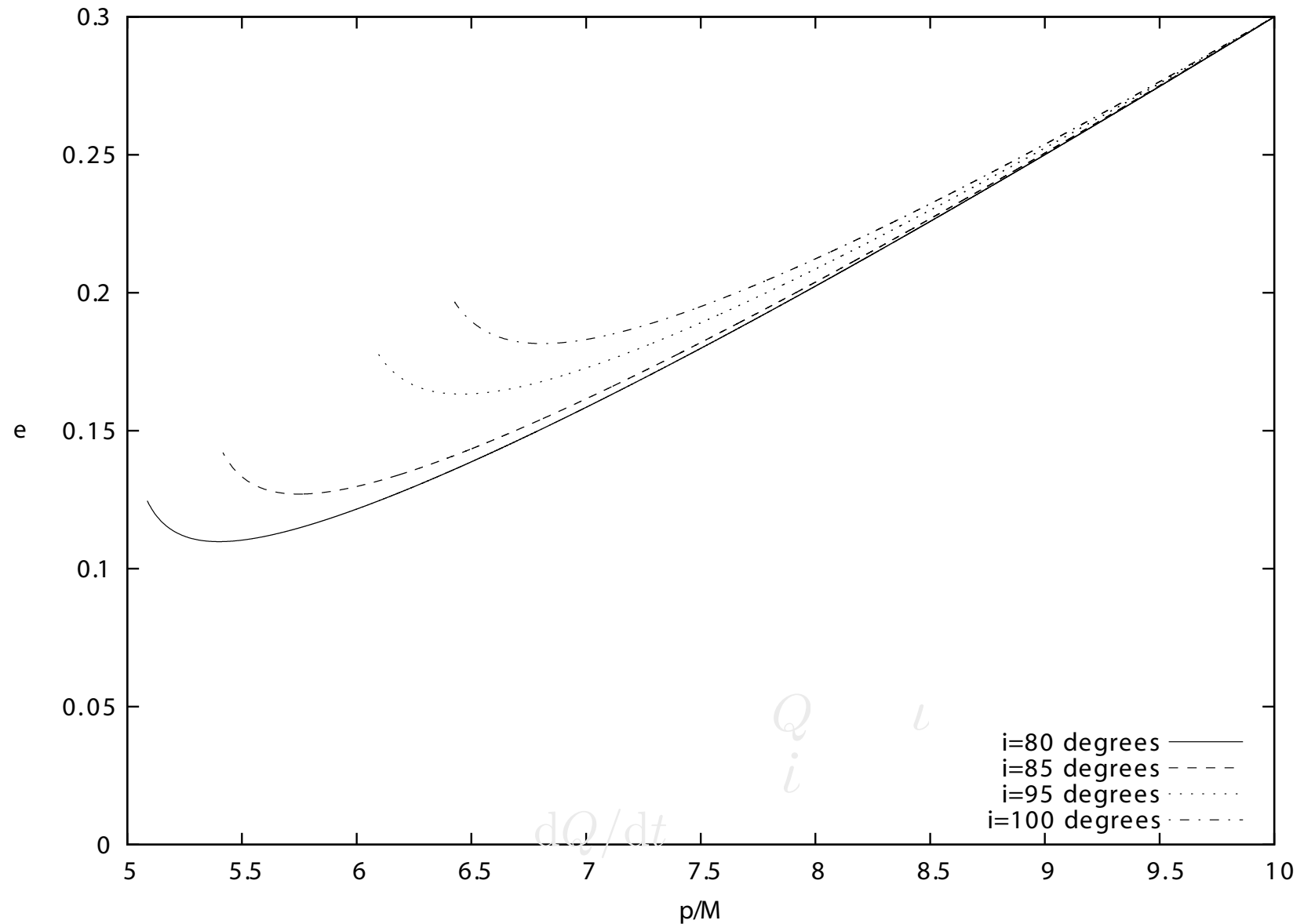
Consistency corrections

- GHK inspirals showed pathological behaviour for near-circular orbits, $de/dt \propto 1/e$.
- This arose from transforming between (E, L_z, Q) and (e, p, ι) - necessary cancellations occur only at PN order of the fluxes.
- Correct by forcing circular orbits to remain circular - use PN expression for \dot{E}, \dot{Q} to determine circular part of \dot{L}_z .
- Constant inclination assumption also gives rise to pathological behaviour for polar orbits since

$$\frac{dQ}{dt} = 2 \sqrt{Q} \frac{\sin \iota}{\cos \iota} \left(\frac{dL_z}{dt} + \sqrt{Q} \frac{1}{\sin^2 \iota} \frac{d\iota}{dt} \right)$$

- Solution is to prescribe evolution of Q not ι . Finiteness at the pole allows us to determine the pieces of i that are non-zero at the pole, and hence improve dQ/dt .

Consistency corrections



2PN Energy and Angular Momentum Fluxes

- Previous corrections are always necessary, but become vanishingly small as the accuracy of the flux expressions improves. Extend to 2PN using results for equatorial orbits (Tagoshi 1995) and for low inclination circular orbits (Shibata et al. 1995). Truncate at 2PN for improved accuracy, and extend to arbitrary inclinations in logical way (e.g., $1 - \iota^2/2 \rightarrow \cos \iota$, $\iota^2 \rightarrow \sin^2 \iota$)

$$\dot{E} = -\frac{32}{5} \frac{\mu^2}{M^2} \left(\frac{M}{p}\right)^5 (1 - e^2)^{3/2} \left[g_1(e) - \left(\frac{a}{M}\right) \left(\frac{M}{p}\right)^{3/2} g_2(e) \cos \iota - \left(\frac{M}{p}\right) g_3(e) \right. \\ \left. + \pi \left(\frac{M}{p}\right)^{3/2} g_4(e) - \left(\frac{M}{p}\right)^2 g_5(e) + \left(\frac{a}{M}\right)^2 \left(\frac{M}{p}\right)^2 g_6(e) - \frac{527}{96} \left(\frac{a}{M}\right)^2 \left(\frac{M}{p}\right)^2 \sin^2 \iota \right]$$

$$\dot{L}_z = -\frac{32}{5} \frac{\mu^2}{M} \left(\frac{M}{p}\right)^{7/2} (1 - e^2)^{3/2} \left[g_7(e) \cos \iota + \left(\frac{a}{M}\right) \left(\frac{M}{p}\right)^{3/2} \{g_8(e) - \cos^2 \iota g_9(e)\} \right. \\ \left. - \left(\frac{M}{p}\right) g_{10}(e) \cos \iota + \pi \left(\frac{M}{p}\right)^{3/2} g_{11}(e) \cos \iota - \left(\frac{M}{p}\right)^2 g_{12}(e) \cos \iota \right. \\ \left. + \left(\frac{a}{M}\right)^2 \left(\frac{M}{p}\right)^2 \cos \iota \left(g_{13}(e) + \frac{45}{8} \cos^2 \iota \right) \right]$$

2PN Carter constant evolution

- Use finiteness at the pole to derive an expression for dQ/dt by cancelling the divergent pieces from dL_z/dt .

$$\begin{aligned}\dot{Q} &= \frac{2\sqrt{Q}\sin\iota}{\cos\iota} \left(\frac{dL_z}{dt} \right)_{2PN} - (\text{terms proportional to } \sec\iota) \\ &= -\frac{64}{5} \frac{\mu^2}{M} \left(\frac{M}{p} \right)^{7/2} \sqrt{Q} \sin\iota (1-e^2)^{3/2} \left[g_9(e) - q \left(\frac{M}{p} \right)^{3/2} \cos\iota g_{10}^b(e) - \left(\frac{M}{p} \right) g_{11}(e) \right. \\ &\quad \left. + \pi \left(\frac{M}{p} \right)^{3/2} g_{12}(e) - \left(\frac{M}{p} \right)^2 g_{13}(e) + q^2 \left(\frac{M}{p} \right)^2 \left(g_{14}(e) - \frac{45}{8} \sin^2\iota \right) \right]\end{aligned}$$

where

$$\begin{aligned}g_9(e) &= 1 + \frac{7}{8}e^2, & g_{10}^b(e) &= \frac{61}{8} + \frac{91}{4}e^2 + \frac{461}{64}e^4, & g_{11}(e) &= \frac{1247}{336} + \frac{425}{336}e^2, \\ g_{12}(e) &= 4 + \frac{97}{8}e^2, & g_{13}(e) &= \frac{44711}{9072} + \frac{302893}{6048}e^2, & g_{14}(e) &= \frac{33}{16} + \frac{95}{16}e^2\end{aligned}$$

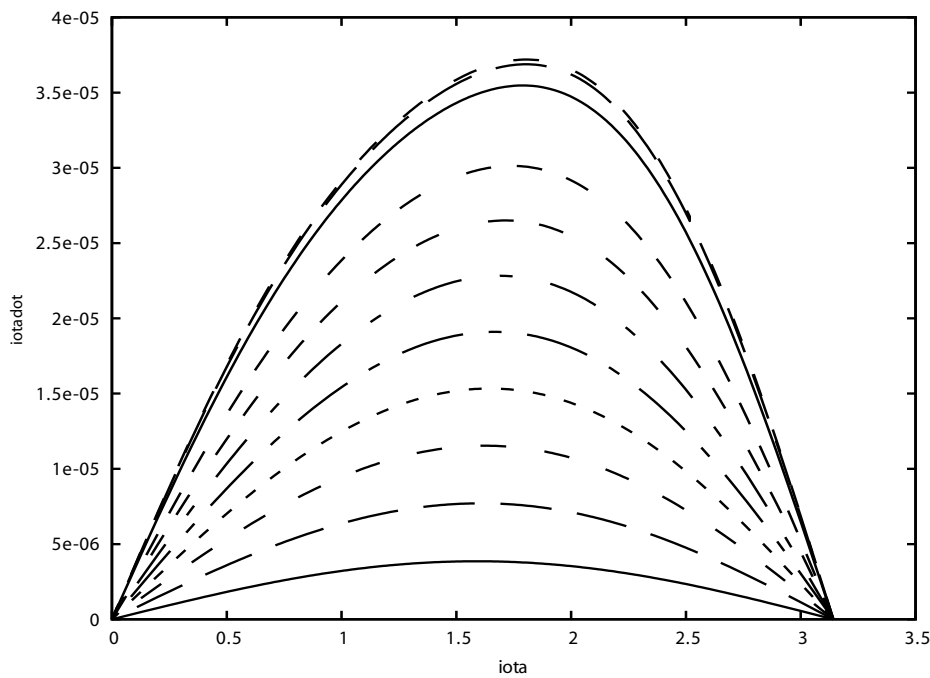
Phase-space evolution - Teukolsky Fit

- Improve evolutions further using accurate perturbative fluxes computed from solution of the Teukolsky equation. So far, have done this for circular, inclined orbits only. Generic orbital data is now available.
- Choose to fit \dot{L}_z and \dot{i} , and derive \dot{E} and \dot{Q} from these. At fixed radius, a fit of the following form works well.

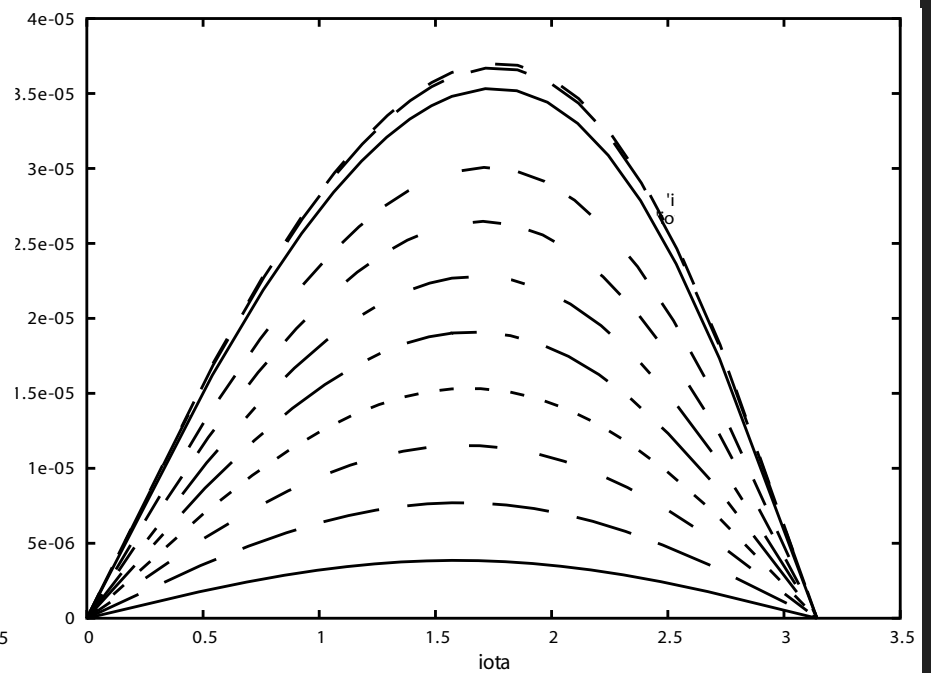
$$\frac{d\iota}{dt} = \frac{32}{5} \frac{\mu^3}{M^4} c_0 \left(\frac{a}{M} \right) \frac{\sin^2 \iota}{\sqrt{Q}} \left(c_1 + \frac{a}{M} c_2 \cos \iota + \left(\frac{a}{M} \right)^2 c_3 \cos^2 \iota \right. \\ \left. + \left(\frac{a}{M} \right)^3 \cos \iota (c_4 + c_5 \cos^2 \iota) + \left(\frac{a}{M} \right)^4 \cos \iota (c_6 + c_7 \cos^2 \iota) \right)$$

- Coefficients are well fit by simple, but long functions of p . Full expressions are given in JG & Glampedakis (2006).

Phase-space evolution - Teukolsky Fit



Kludge



Teukolsky

Conservative Corrections

- Can include conservative effects in the kludge by adding corrections into the geodesic equations, e.g.,

$$\frac{d\phi}{dt} = 2\pi (\Omega_{\text{geo}} + \delta\Omega(p, e, \iota))$$

- Conservative piece is gauge dependent. Our aim is to reproduce observed waveforms as well as possible, so we determine the corrections by considering gravitational wave observables - Ω and $d\Omega/dt$ measured by an observer at infinity.
- Make progress by comparing to pN results (Huerta & JG 2009)

$$M \frac{d\phi}{dt} = \frac{1}{(p/M)^{3/2} + q} \left\{ 1 + \eta \left(d_0 + d_1 \left(\frac{M}{p} \right) + (d_{1.5} + q l_{1.5}) \left(\frac{M}{p} \right)^{3/2} + d_2 \left(\frac{M}{p} \right)^2 \right) \right\}$$

where $q = a/M$ $\eta = m/M$

$$d_0 = \frac{1}{8}, \quad d_1 = \frac{1975}{896}, \quad l_{1.5} = -\frac{191}{200}, \quad d_2 = \frac{1152193}{451584}$$

Waveform Generation

- Define pseudo-Cartesian coordinates from Boyer-Lindquist (r, θ, ϕ) by

$$x = r \sin \theta \cos \phi, \quad y = r \sin \theta \sin \phi, \quad z = r \cos \theta$$

- Construct flat-space quadrupole moment tensor based on these coordinates

$$\mathcal{I}^{ij} = x^i(t) x^j(t) - \frac{1}{3} \delta^{ij} r^2(t), \quad h^{ij} = \frac{2}{r} \frac{d^2}{dt^2} \mathcal{I}^{ij}$$

- This prescription generates purely quadrupolar waveforms. Can generate waveforms including higher multipoles in a similar way – quadrupole/octupole waveforms or Press waveforms (weak field, fast motion approximation) (Babak, Fang, JG et al. 2007).

$$\bar{h}^{jk}(t, \mathbf{x}) = \frac{2}{r} \frac{d^2}{dt^2} \int [(\mathcal{T}^{00} - 2\mathcal{T}^{0l} n_l + \mathcal{T}^{lm} n_l n_m) x'^j x'^k]_{t'=t-|\mathbf{x}-\mathbf{x}'|} d^3 x'$$

Tests - Comparison to Teukolsky Data

- Compare fluxes to Teukolsky-based results. For instance, circular orbits with inclination $\iota = \pi/3$

$\frac{p}{M}$	$\frac{a}{M}$	$ \dot{E}^T - \dot{E}^K /\dot{E}^T$	$ \dot{L}_z^T - \dot{L}_z^K /\dot{L}_z^T$	$ i^T - i^K /i^T$
7	0.05	0.0018	0.0018	0.0027
7	0.95	0.0013	0.0018	0.0029
100	0.05	0.00025	0.00025	0.0018
100	0.95	0.00022	0.00018	0.0008

Tests - Comparison to Teukolsky Data

a/M	p/M	e	ι	$(M/\mu)^2 \dot{E}$		$(M/\mu^2) L_z$		$(M^3/\mu^2) i$	
				Teuk	Hybrid	Teuk	Hybrid	Teuk	Hybrid
0.05	100	0	60	-6.237×10^{-10}	-6.237×10^{-10}	-3.119×10^{-7}	-3.119×10^{-7}	6.706×10^{-12}	6.718×10^{-12}
0.95	100	0	60	-6.219×10^{-10}	-6.219×10^{-10}	-3.122×10^{-7}	-3.122×10^{-7}	1.267×10^{-10}	1.268×10^{-10}
0.05	7	0	60	-3.951×10^{-4}	-3.958×10^{-4}	-3.697×10^{-3}	-3.704×10^{-3}	1.104×10^{-5}	1.107×10^{-5}
0.95	7	0	60	-3.055×10^{-4}	-3.051×10^{-4}	-3.368×10^{-3}	-3.362×10^{-3}	1.706×10^{-4}	1.701×10^{-4}
0.5	5	0.1	0	-1.813×10^{-3}	-1.787×10^{-3}	-2.063×10^{-2}	-2.019×10^{-2}	0	0
0.5	5	0.2	0	-2.087×10^{-3}	-1.951×10^{-3}	-2.208×10^{-2}	-2.019×10^{-2}	0	0
0.5	5	0.3	0	-2.601×10^{-3}	-2.170×10^{-3}	-2.480×10^{-2}	-2.001×10^{-2}	0	0
0.99	2	0.1	0	-4.4067×10^{-2}	-3.938×10^{-2}	-1.657×10^{-1}	-1.204×10^{-1}	0	0
0.99	2	0.2	0	-4.723×10^{-2}	-4.702×10^{-2}	-1.700×10^{-1}	-7.249×10^{-2}	0	0
0.99	2	0.3	0	-5.444×10^{-2}	-5.084×10^{-2}	-1.771×10^{-1}	2.395×10^{-3}	0	0
0.99	3	0.1	0	-1.083×10^{-2}	-1.096×10^{-2}	-6.583×10^{-2}	-6.293×10^{-2}	0	0
0.99	3	0.2	0	-1.153×10^{-2}	-1.259×10^{-2}	-6.684×10^{-2}	-6.001×10^{-2}	0	0
0.99	3	0.3	0	-1.262×10^{-2}	-1.439×10^{-2}	-6.825×10^{-2}	-5.473×10^{-2}	0	0
0.99	11	0.1	180	-4.961×10^{-5}	-4.932×10^{-5}	1.736×10^{-3}	1.711×10^{-3}	0	0
0.99	11	0.2	180	-5.589×10^{-5}	-5.248×10^{-5}	1.821×10^{-3}	1.709×10^{-3}	0	0
0.99	11	0.3	180	-6.657×10^{-5}	-5.687×10^{-5}	1.963×10^{-3}	1.695×10^{-3}	0	0
0.9	6	0.1	40.192 285	-6.145×10^{-4}	-6.196×10^{-4}	-7.551×10^{-3}	-7.534×10^{-3}	0	2.611×10^{-4}
0.9	6	0.3	40.176 668	-7.209×10^{-4}	-7.512×10^{-4}	-7.641×10^{-3}	-7.632×10^{-3}	0	3.197×10^{-4}
0.9	6	0.5	40.145 475	-8.654×10^{-4}	-8.475×10^{-4}	-7.670×10^{-3}	-7.143×10^{-3}	0	3.768×10^{-4}
0.9	6	0.1	80.046 323	-8.060×10^{-4}	-8.007×10^{-4}	-3.427×10^{-3}	-3.395×10^{-3}	0	4.371×10^{-4}
0.9	6	0.3	80.042 690	-1.086×10^{-3}	-9.879×10^{-4}	-4.023×10^{-3}	-3.659×10^{-3}	0	5.051×10^{-4}
0.9	6	0.5	80.035 363	-1.685×10^{-3}	-1.163×10^{-3}	-5.133×10^{-3}	-3.761×10^{-3}	0	5.602×10^{-4}

Tests - Comparison to Teukolsky Data

- Compare fluxes to Teukolsky-based results. For instance, circular orbits with inclination $\iota = \pi/3$

$\frac{p}{M}$	$\frac{a}{M}$	$ \dot{E}^T - \dot{E}^K /\dot{E}^T$	$ \dot{L}_z^T - \dot{L}_z^K /\dot{L}_z^T$	$ i^T - i^K /i^T$
7	0.05	0.0018	0.0018	0.0027
7	0.95	0.0013	0.0018	0.0029
100	0.05	0.00025	0.00025	0.0018
100	0.95	0.00022	0.00018	0.0008

- Compute overlaps between Teukolsky and kludge waveforms for geodesic orbits

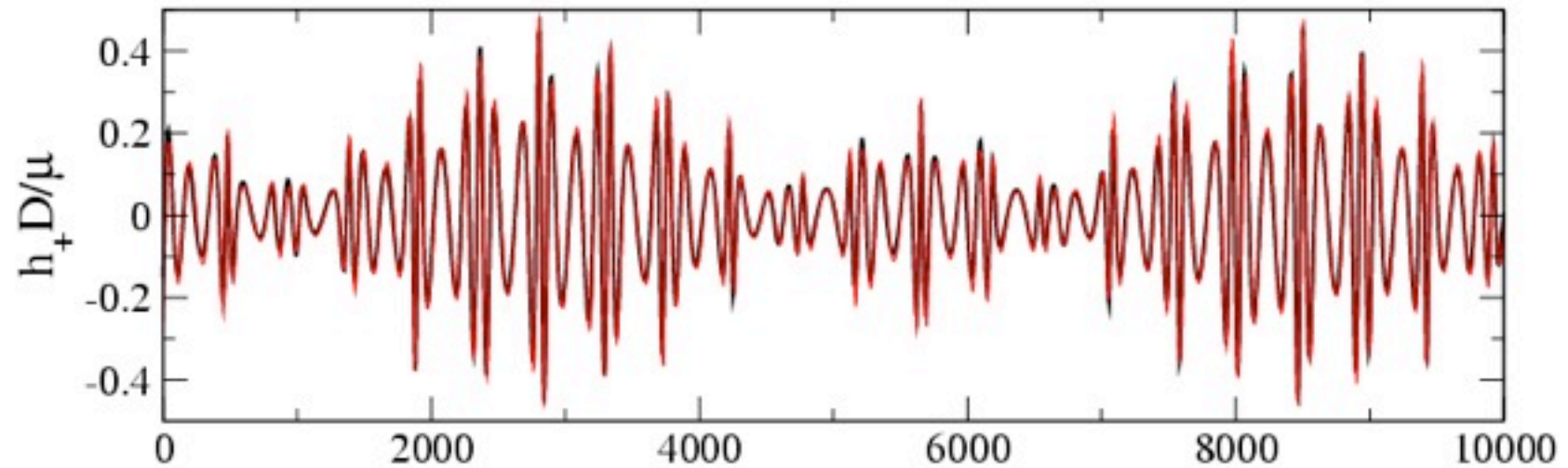
p	e	a	overlap	p	ι	a	overlap
1.7	0.1	0.99	0.741	5	30	0.5	0.990
1.7	0.3	0.99	0.500	5	30	0.99	0.973
2.5	0.1	0.99	0.827	5	60	0.99	0.888
2.5	0.5	0.99	0.651	10	30	0.5	0.990
5.1	0.5	0.5	0.967	10	30	0.99	0.982
10	0.3	-0.99	0.966	10	60	0.99	0.937

Tests - Waveform Comparisons

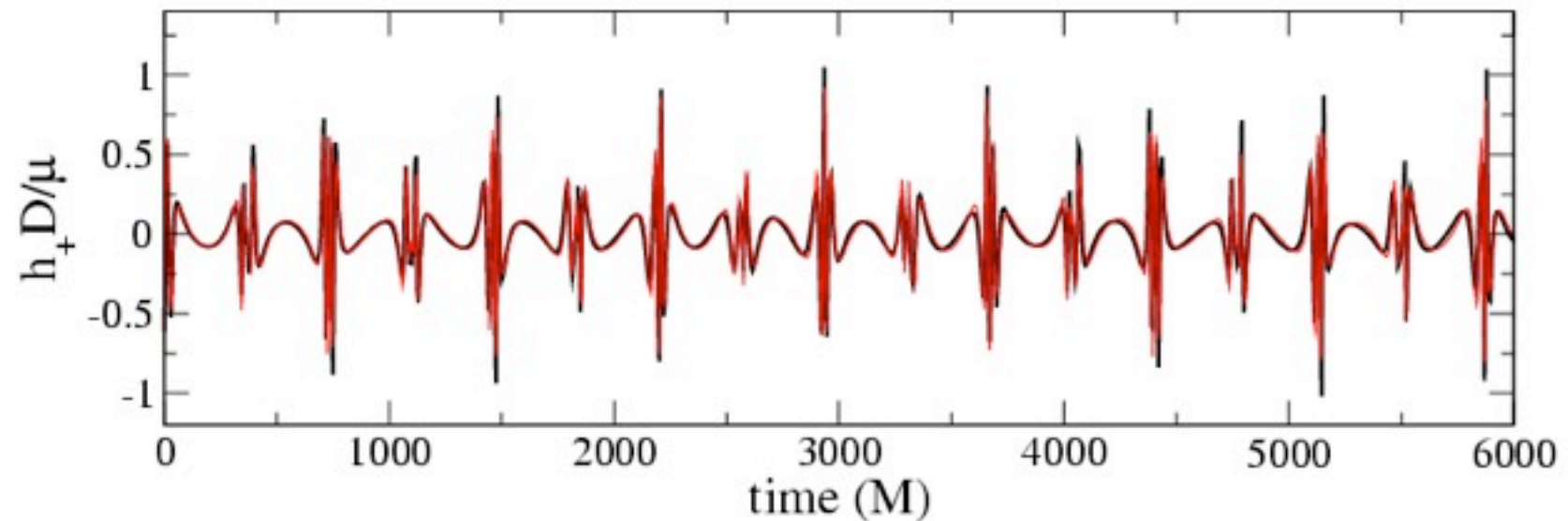
- Compare kludge waveforms to Teukolsky waveforms for geodesics
- agreement is remarkable, even in the strong field.

Tests - Waveform Comparisons

$a=0.9M$, $p = 12M$, $e = 0.3$, $\iota = 140(\text{deg})$, $\theta_d = 60(\text{deg})$



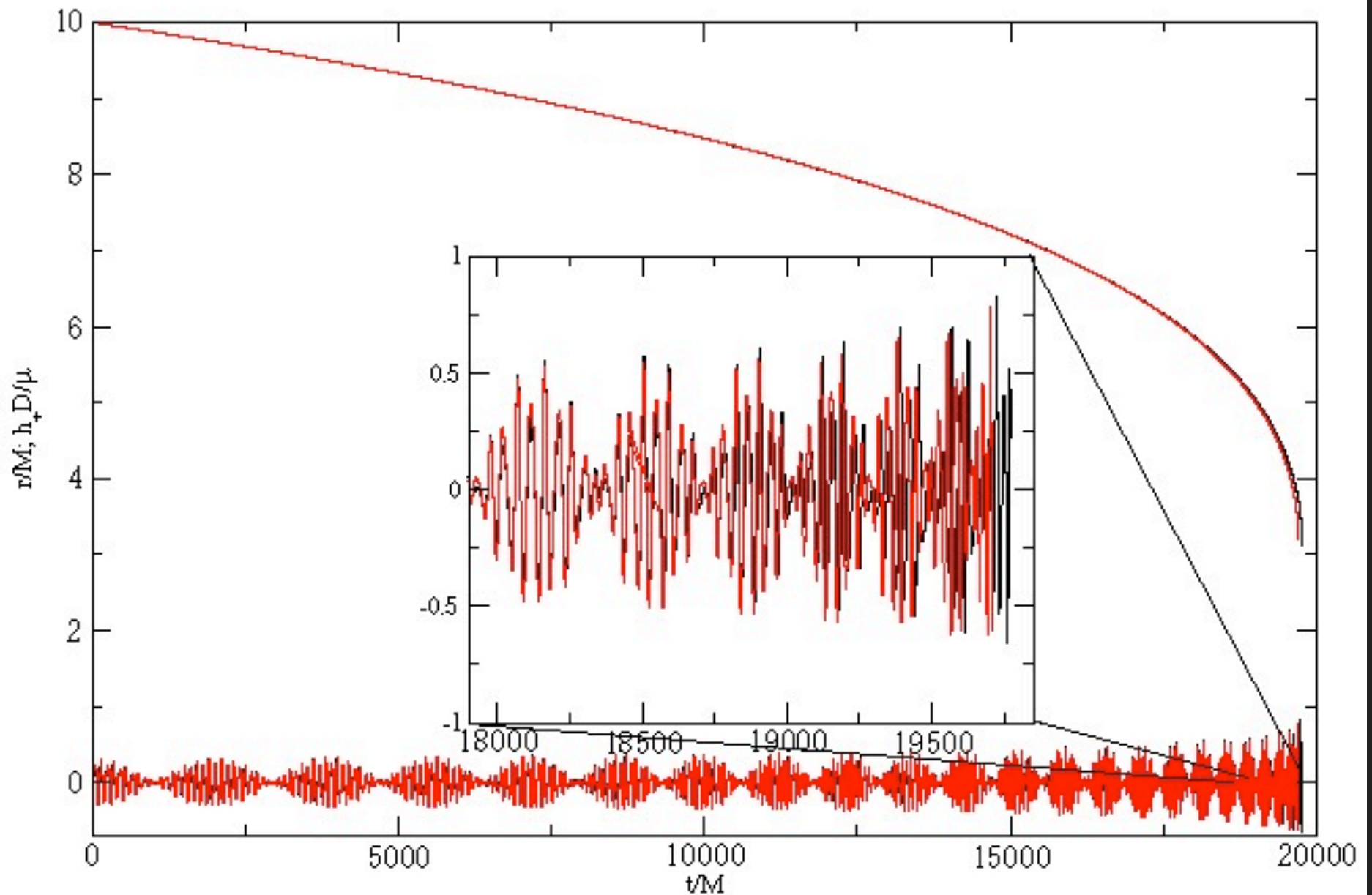
$a = 0.9M$, $p = 6M$, $e = 0.7$, $\iota = 60(\text{deg})$, $\theta_d = 90(\text{deg})$



Tests - Waveform Comparisons

- Compare kludge waveforms to Teukolsky waveforms for geodesics - agreement is remarkable, even in the strong field.
- Have also done comparisons for *inspiral* waveforms, for circular-inclined inspirals, for which the phase-space evolution is most accurate. Agreement is very good until the last few cycles before plunge.

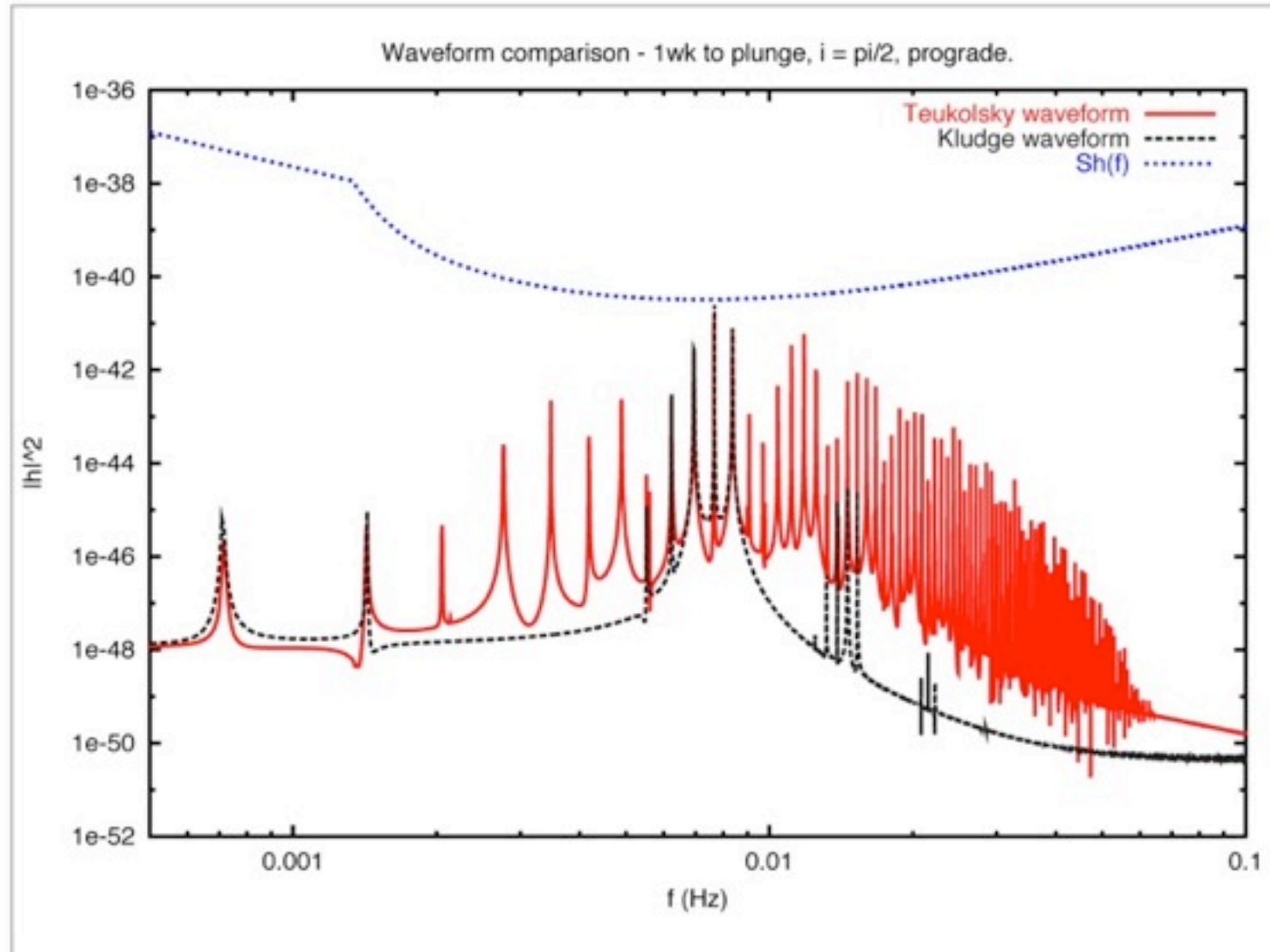
Tests - Waveform Comparisons



Tests - Waveform Comparisons

- Compare kludge waveforms to Teukolsky waveforms for geodesics - agreement is remarkable, even in the strong field.
- Have also done comparisons for *inspiral* waveforms, for circular-inclined inspirals, for which the phase-space evolution is most accurate. Agreement is very good until the last few cycles before plunge.
- Comparison of spectrum of radiation to Teukolsky results indicates that the frequencies represented in the kludge spectrum are correct but many modes are absent. However, these modes are generally suppressed until the very end.

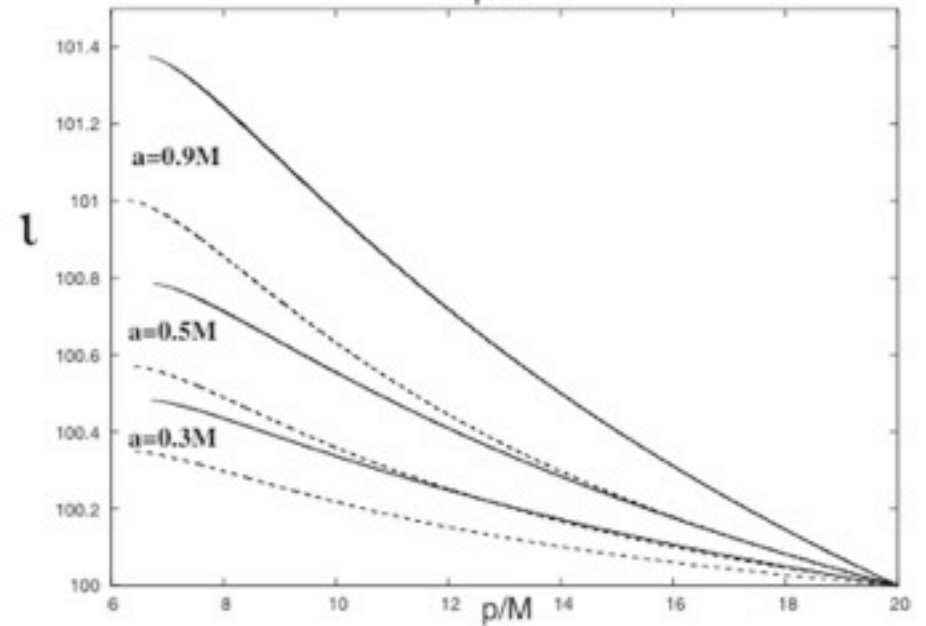
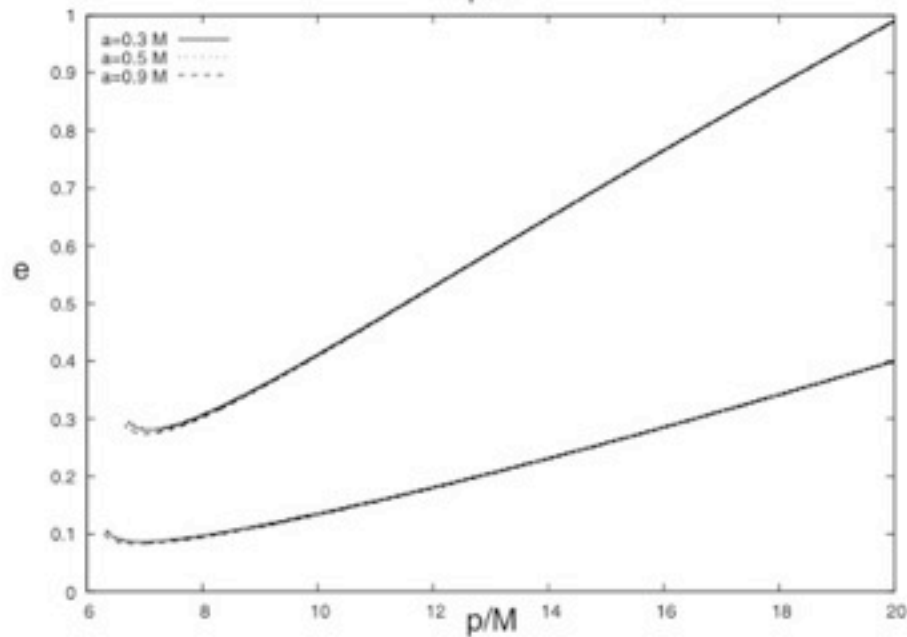
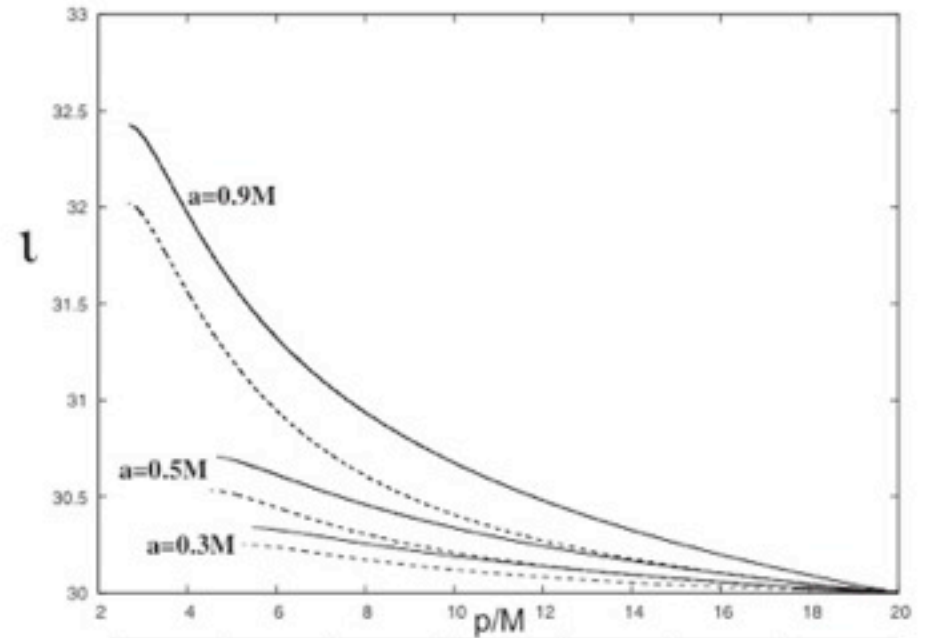
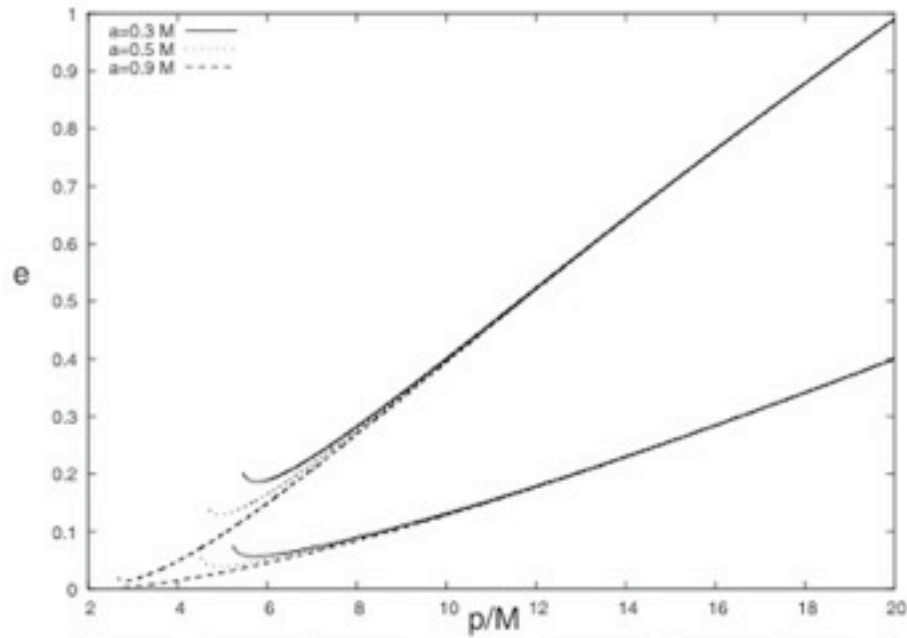
Tests - Waveform Comparisons



Applications of kludge waveforms

- **Compute inspirals** - generate trajectories and waveforms for generic inspirals.

Applications of kludge waveforms



Applications of kludge waveforms

- **Compute inspirals** - generate trajectories and waveforms for generic inspirals.
- **Compute EMRI SNRs** - use to estimate event rates for LISA/NGO; explore scientific applications of EMRI observations.

M	m	S/N(AET)						S/N(X)				
		(1wk)	(1mo)	(3mo)	(1yr)	(3yr)	(5yr)	(1wk)	(1mo)	(3mo)	(1yr)	(3yr)
$3 \cdot 10^5$	0.6	1.1	3.0	5.1	10.2	16.8	20.4	0.6	1.6	2.2	5.8	10.2
$3 \cdot 10^5$	10	27.8	60.3	80.4	119.0	149.0	162.0	16.6	38.0	48.8	74.7	95.4
$3 \cdot 10^5$	100	277.0	440.0	508.0	591.0	626.0	633.0	188.0	300.0	338.0	391.0	414.0
10^6	0.6	3.7	7.3	10.0	18.5	29.0	34.9	2.5	4.9	6.3	12.0	19.0
10^6	10	58.2	109.0	140.0	205.0	252.0	271.0	40.5	75.5	92.9	136.0	168.0
10^6	100	477.0	752.0	860.0	989.0	1060.0	1090.0	338.0	532.0	595.0	678.0	727.0
$3 \cdot 10^6$	0.6	3.1	6.0	8.0	14.1	21.2	24.9	2.2	4.2	5.4	9.5	14.3
$3 \cdot 10^6$	10	45.7	81.8	102.0	138.0	158.0	164.0	32.7	57.8	69.8	93.9	107.0
$3 \cdot 10^6$	100	344.0	508.0	559.0	590.0	601.0	604.0	244.0	360.0	391.0	411.0	418.0

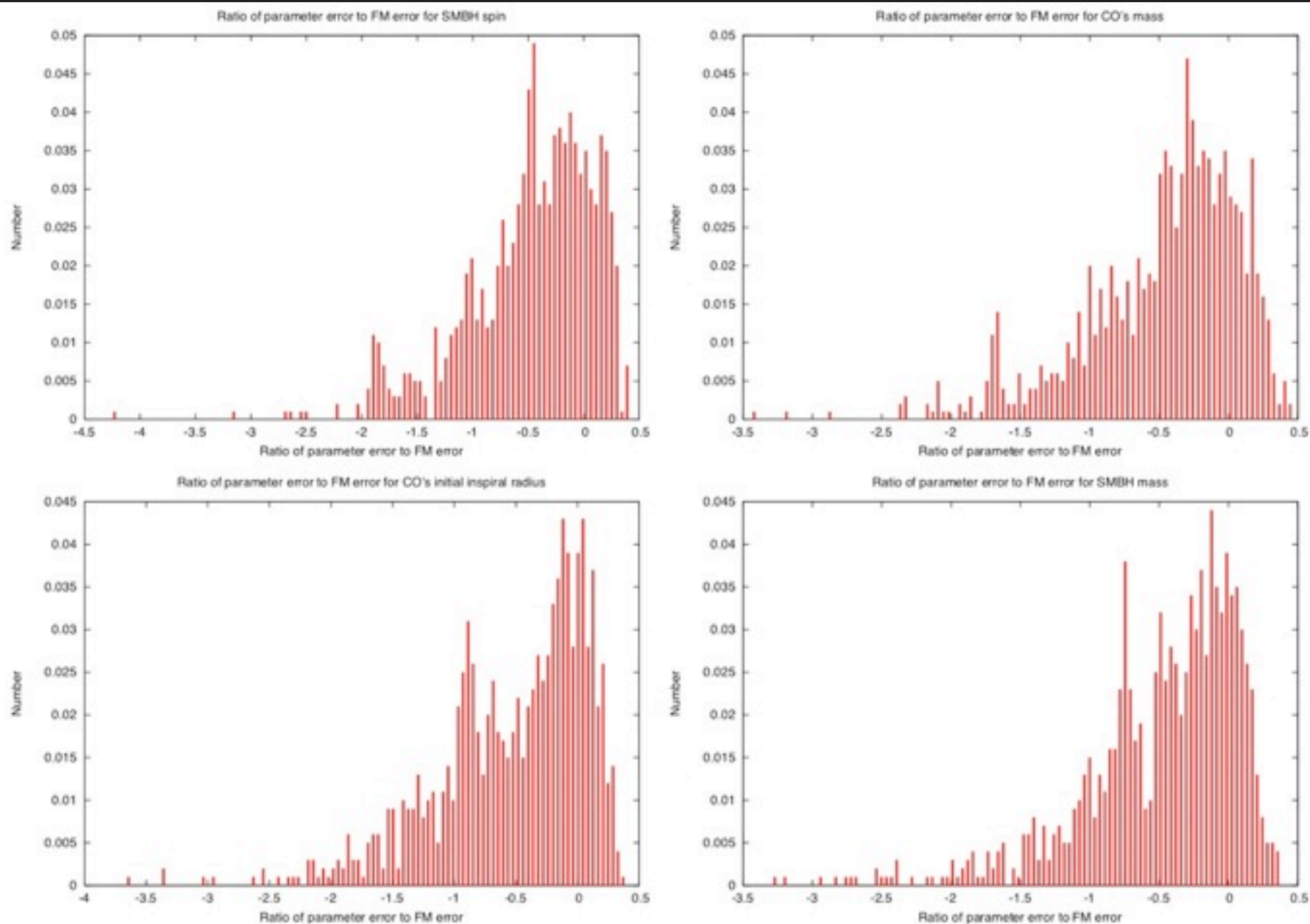
Applications of kludge waveforms

- **Compute inspirals** - generate trajectories and waveforms for generic inspirals.
- **Compute EMRI SNRs** - use to estimate event rates for LISA/NGO; explore scientific applications of EMRI observations.
- **Scope out data analysis for LISA/NGO** - analytic kludge waveforms used for Mock LISA Data Challenges; numerical kludge used to explore semi-coherent search techniques. Also used to estimate parameter estimation accuracies.

Applications of kludge waveforms

- **Compute inspirals** - generate trajectories and waveforms for generic inspirals.
- **Compute EMRI SNRs** - use to estimate event rates for LISA/NGO; explore scientific applications of EMRI observations.
- **Scope out data analysis for LISA/NGO** - analytic kludge waveforms used for Mock LISA Data Challenges; numerical kludge used to explore semi-coherent search techniques. Also used to estimate parameter estimation accuracies.
- **Assess importance of conservative corrections** - estimate dephasing and systematic error that arises from omitting conservative corrections to the phase evolution. Find corrections are marginally important for black hole inspirals, ignorable for WD/NS inspirals.

Applications of kludge waveforms



Self-forced Evolution

JG, E. Flanagan, S. Drasco, T. Hinderer & S. Babak, PRD 83 044037 (2011)

Method of Osculating Elements

- Method to solve for the evolution of a conservative system under a perturbing force

$$\frac{Du^\mu}{D\tau} = \frac{d^2x^\mu}{d\tau^2} - f_{\text{geo}}^\mu = \delta f^\mu$$

- Identify orbit at any time with the geodesic of the unperturbed system ($\delta f^\mu = 0$) that passes through the *same position* with the *same velocity*. In this way we describe the trajectory using *osculating orbital elements* $I(t) = \{E(t), L_z(t), Q(t), \psi_0(t), \chi_0(t), \phi_0(t)\}$
- The osculating elements evolve as

$$\dot{I} = \nabla_r I \cdot \dot{\mathbf{r}} + \nabla_v I \cdot \dot{\mathbf{v}} = \nabla_v I \cdot \delta f$$

- Reduces second-order differential equations to a set of coupled first-order equations. Valid for *any perturbing force*, but method is most useful when the force is small - use it to construct an averaged evolution.

Osculating Elements - example

- Can illustrate osculating element techniques using a forced damped harmonic oscillator

$$\ddot{x} + x + \beta x^3 = \epsilon a_{\text{ext}} \quad a_{\text{ext}} = -\gamma \dot{x} + \delta x^2$$

- For the unperturbed motion, we have an energy integral that defines an amplitude parameter

$$\frac{1}{2}a^2 + \frac{1}{4}\beta a^4 = \frac{1}{2}\dot{x}^2 + \frac{1}{2}x^2 + \frac{1}{4}\beta x^4$$

- and we can write the solution in a simple amplitude/phase form

$$x = a \cos(\Psi - \Psi_0) = a \cos \psi$$

$$\dot{\psi} = \sqrt{1 + \beta a^2(1 + \cos^2 \psi)}/2$$

$$\dot{a} = 0$$

$$\dot{x} = -a \sin \psi \sqrt{1 + \beta a^2(1 + \cos^2 \psi)}/2$$

Osculating Elements - example

- In the presence of a forcing term, the amplitude parameter changes slowly with time. The osculating amplitude is given directly by the energy equation

$$\frac{1}{2}a^2 + \frac{1}{4}\beta a^4 = \frac{1}{2}\dot{x}^2 + \frac{1}{2}x^2 + \frac{1}{4}\beta x^4$$

- Differentiation of this equation gives an equation for the evolution of the amplitude

$$(a + \beta a^3)\dot{a} = \epsilon \dot{x} a_{\text{ext}} \quad \Rightarrow \quad \dot{a} = -\epsilon \sqrt{1 + \beta a^2(1 + \cos^2 \psi)/2} \frac{\sin \psi a_{\text{ext}}}{1 + \beta a^2}$$

- Differentiation of the orbit equation, with a time varying amplitude, gives $\dot{x} = \dot{a} \cos \psi - a \sin \psi \dot{\psi}$
- Applying the osculating element condition again, we find

$$\dot{\psi} = \sqrt{1 + \beta a^2(1 + \cos^2 \psi)/2} \left(1 - \epsilon \frac{\cos \psi a_{\text{ext}}}{a(1 + \beta a^2)} \right)$$

Osculating Elements - example

- Can also use an elliptic integral solution to unforced motion

$$x = k \sqrt{\frac{2(1 - k^2)}{\beta(1 - 2k^2)}} \text{sd}(u; k) \quad u = \frac{(t - t_0)}{\sqrt{1 - 2k^2}}$$

$$k^2 = \frac{\sqrt{1 + 2E\beta} - 1}{2\sqrt{1 + 2E\beta}} \quad E = a^2 + \frac{1}{2}\beta a^4$$

- Find osculating solution is

$$\frac{dk}{dt} = \epsilon a_{\text{ext}}(x, \dot{x}) (1 - 2k^2)^2 \sqrt{\frac{\beta}{2}(1 - k^2)} \frac{\partial \text{sd}}{\partial u}$$

$$\frac{du}{dt} = \frac{1}{\sqrt{1 - 2k^2}} - \epsilon a_{\text{ext}}(x, \dot{x}) (1 - 2k^2) \sqrt{\frac{\beta}{2}(1 - k^2)} \times \left[\frac{1 - 2k^2 + 2k^4}{k(1 - k^2)(1 - 2k^2)} \text{sd}(u; k) + \frac{\partial \text{sd}}{\partial k} \right]$$

Osculating Elements - example

- Construct averaged solution by writing

$$\begin{aligned}\dot{u} &= \omega(u, k) + \epsilon g^{(1)}(u, k) + O(\epsilon^2) \\ \dot{k} &= \epsilon G^{(1)}(u, k) + O(\epsilon^2)\end{aligned}$$

- defining an averaging operation

$$\langle f(u, k) \rangle_k = \frac{1}{4\mathbf{K}(k)} \int_0^{4\mathbf{K}(k)} du f(u, k)$$

- and computing the average of the leading order terms

$$\begin{aligned}\bar{\omega} &= \langle \omega \rangle_k = \omega \\ \bar{G}^{(1)} &= \langle G^{(1)} \rangle_k = \gamma(1 - 2k^2) \left[\left(\frac{2}{3} \frac{2 - k^2}{k} - \frac{1}{k} \right) \frac{\mathbf{E}(k)}{\mathbf{K}(k)} - \frac{1 - k^2}{3k} \right]\end{aligned}$$

- Then construct average evolution as a function of $\tilde{t} = \epsilon t$

$$\frac{d\chi^{(0)}}{d\tilde{t}} = \bar{\omega}(k^{(0)}(\tilde{t})), \quad \frac{dk^{(0)}}{d\tilde{t}} = \bar{G}^{(1)}(k^{(0)}(\tilde{t}))$$

Osculating Elements - example

- In general, the phase is then given by

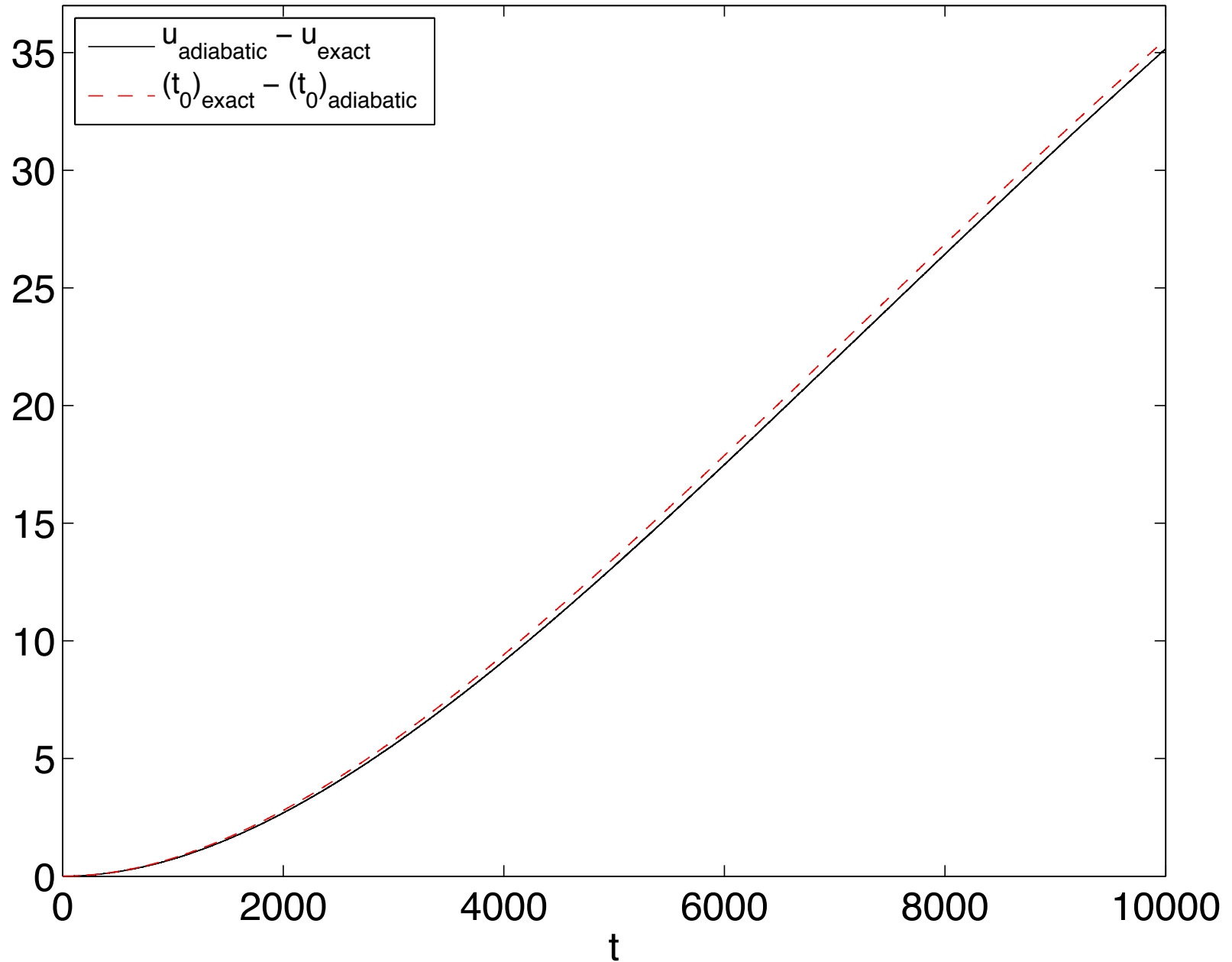
$$u(t, \epsilon) = \Xi \left[\frac{1}{\epsilon} \chi^{(0)}(\epsilon t), k^{(0)}(\epsilon t) \right] \quad \frac{\chi}{4\mathbf{K}(k)} = \frac{\int_0^{\Xi(\chi, a)} \frac{du}{\omega(u, a)}}{\int_0^{4\mathbf{K}(k)} \frac{du}{\omega(u, a)}}$$

- which simplifies greatly in this case to

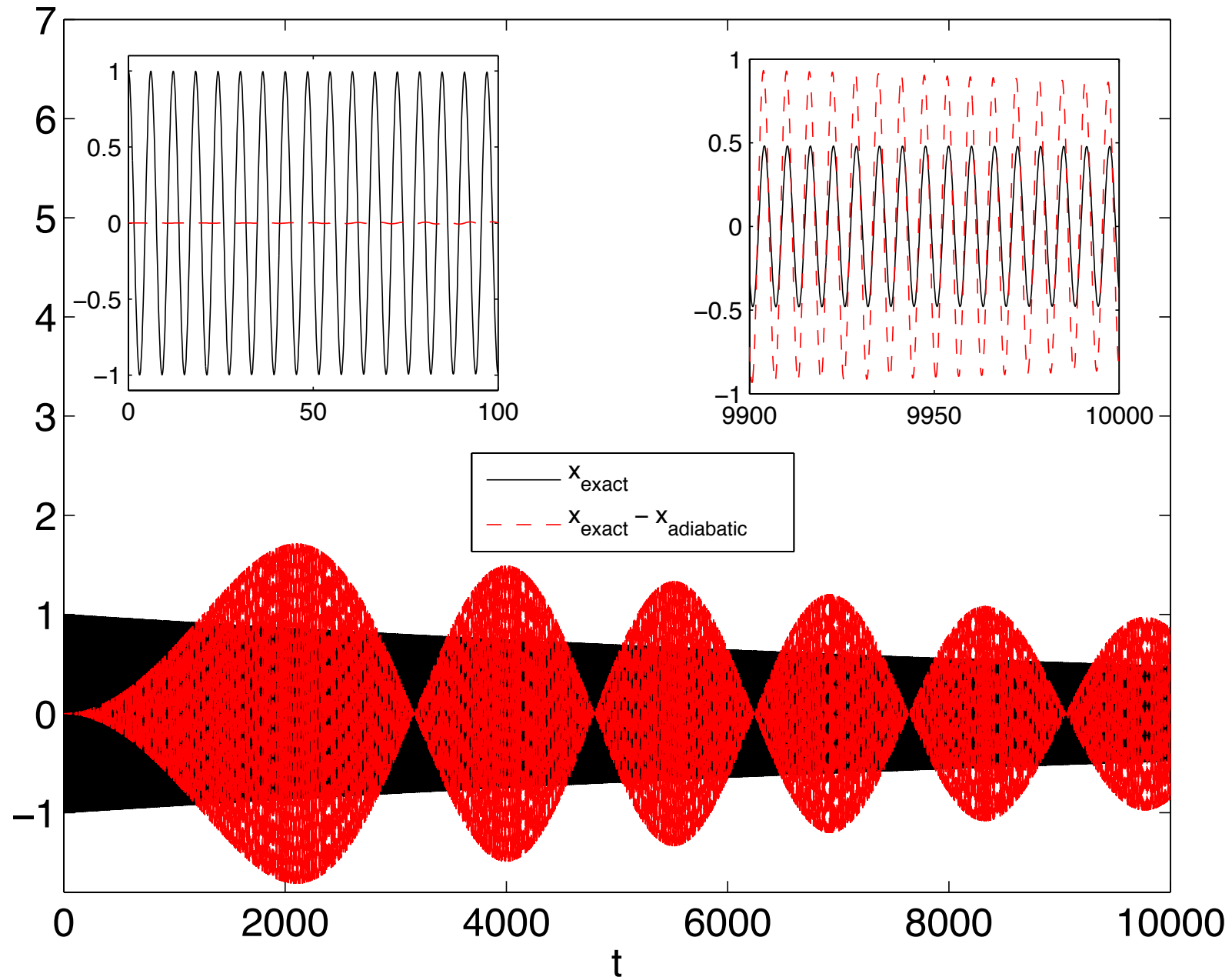
$$u(t, \epsilon) = \frac{1}{\epsilon} \chi^{(0)}(\epsilon t)$$

- Exact and averaged evolution show close agreement in the energy parameter, k , for a time of $O(1/\epsilon^2)$, while phase starts to disagree after a time of $O(1/\epsilon)$. To be expected from scaling of terms that are omitted in the averaged solution.

Osculating Elements - example



Osculating Elements - example



Black Hole Osculating Orbits

- To generate osculating evolutions for Kerr black hole spacetimes, we need a convenient parameterisation of the orbit.
- Use orbital constants (E, L_z, Q) or (p, e, ι) and two phase angles defined by writing

$$r = \frac{p}{1 + e \cos(\psi - \psi_0)} \quad \cos^2 \theta = \cos^2 \theta_{\max} \cos^2(\chi - \chi_0)$$

- The coordinates t and ϕ are not oscillatory. Osculating element equations for $t - t_0$ and $\phi - \phi_0$ are equivalent to integrating the geodesic equations for these coordinates with the evolving orbit on the right hand side.
- Final equation follows from orthogonality of acceleration to velocity, i.e.,

$$u_\mu \delta f^\mu = 0$$

Black Hole Osculating Orbits

- Equations for (E, L_z, Q) are most easily derived from covariant equations of motion

$$\dot{E} = -\delta f_t$$

$$\dot{L}_z = \delta f_\phi$$

$$\dot{K} = \dot{E} \frac{2}{\Delta} (\varpi^4 E - a\varpi^2 L_z) + \dot{L}_z \frac{2}{\Delta} (a^2 L_z - a\varpi^2 E) - 2\Delta u_r \delta f_r$$

- where $K = Q + (L_z - aE)^2$, $\varpi^2 = r^2 + a^2$
- Equations for phase constants appear singular at turning points

$$\dot{\psi}_0 = -\frac{1}{\partial r / \partial \psi_0} \left(\frac{\partial r}{\partial E} \dot{E} + \frac{\partial r}{\partial L_z} \dot{L}_z + \frac{\partial r}{\partial Q} \dot{Q} \right)$$

$$\dot{\chi}_0 = -\frac{1}{\partial \theta / \partial \chi_0} \left(\frac{\partial \theta}{\partial E} \dot{E} + \frac{\partial \theta}{\partial L_z} \dot{L}_z + \frac{\partial \theta}{\partial Q} \dot{Q} \right)$$

Black Hole Osculating Orbits

- Singularity is not real. If we take the radial geodesic equation

$$\Sigma^2 \dot{r}^2 = V_r(r, L_z, E, Q)$$

- differentiate with respect to (E, L_z, Q) and then combine the expressions we find an alternative expression for $\dot{\psi}_0$

$$\dot{\psi}_0 = 2 \frac{\dot{\psi}_{\text{geo}}}{\partial V_r / \partial r} \left[\Sigma^2 \left(\dot{E} \frac{\partial \dot{r}}{\partial E} + \dot{L}_z \frac{\partial \dot{r}}{\partial L_z} + \dot{Q} \frac{\partial \dot{r}}{\partial Q} \right) + 2 \Sigma r \dot{r} \left(\dot{E} \frac{\partial r}{\partial E} + \dot{L}_z \frac{\partial r}{\partial L_z} + \dot{Q} \frac{\partial r}{\partial Q} \right) - 2 \Sigma a^2 \cos \theta \sin \theta \dot{r} \left(\dot{E} \frac{\partial \theta}{\partial E} + \dot{L}_z \frac{\partial \theta}{\partial L_z} + \dot{Q} \frac{\partial \theta}{\partial Q} \right) - \Sigma^2 \delta f^r \right]$$

- in which $\Sigma^2 = r^2 + a^2 \cos^2 \theta$. We can derive a similar expression for $\dot{\chi}_0$ using the polar geodesic equation. These equations appear singular at zeros of $\partial V_r / \partial r$, but these are also not real singularities. Can explicitly simplify expressions or use different expressions near and far from turning points.

Black Hole Osculating Orbits - Tetrad Formulation

- Manifestly non-singular form of the equations can also be found by decomposing the force on the Kinnersley tetrad

$$\vec{\delta f} = -\delta f_n \vec{l} - \delta f_l \vec{n} + \delta f_m^* \vec{m} + \delta f_m \vec{m}^*$$

$$R_f = \frac{1}{\sqrt{2}}(\delta f_m + \delta f_m^*)$$

$$I_f = \frac{i}{\sqrt{2}}(\delta f_m - \delta f_m^*)$$

- The independent acceleration components can be written as

$$\mathcal{A}_I = r R_f + a I_f \cos \theta$$

$$\mathcal{A}_{II} = r I_f - a R_f \cos \theta$$

$$\mathcal{A}_{III} = R_u R_f + I_u I_f$$

- and we find the evolution of the orbital constants is given by

$$\frac{dE}{d\lambda} = \frac{u_r a_n \Delta}{u_n} - \frac{\Delta \mathcal{A}_{III}}{2u_n} - a \sin \theta \mathcal{A}_{II} \quad \frac{dK}{d\lambda} = 2\Sigma^2 \mathcal{A}_{III}$$

$$\frac{dL_z}{d\lambda} = \frac{a \sin^2 \theta u_r a_n \Delta}{u_n} - \frac{a \sin^2 \theta \Delta \mathcal{A}_{III}}{2u_n} - \varpi^2 \sin \theta \mathcal{A}_{II}$$

Black Hole Osculating Orbits - Tetrad Formulation

- The evolution of the phase constants can be found to be

$$\frac{d\chi_\theta}{d\lambda} = \sqrt{\beta(z_+ - z_-)} \left[1 + \frac{(1 - z_-)\Sigma\mathcal{A}_I \cos \chi_\theta}{\beta\sqrt{z_-}(z_+ - z_-) \sin \theta} \right] + \frac{\cos \chi_\theta \sin \chi_\theta \mathcal{H}a\Delta(\mathcal{A}_{III} - 2u_r a_n)}{2(z_+ - z_-)\beta u_n} + \frac{\cos \chi_\theta \sin \chi_\theta \mathcal{G}\mathcal{A}_{II}}{\beta(z_+ - z_-)}$$

$$\begin{aligned} \frac{d\psi_r}{d\lambda} = & \mathcal{P} + \frac{\mathcal{C}\mathcal{A}_{III} \sin \psi_r}{2(1 + e \cos \psi_r)u_n} + \frac{\mathcal{D}\Sigma\mathcal{A}_{III}\mathcal{P}}{2(1 + e \cos \psi_r)^2 u_n} \\ & - \frac{a\mathcal{E} \sin \theta \sin \psi_r \mathcal{A}_{II}}{1 + e \cos \psi_r} + \frac{\mathcal{P}a_n}{u_n(1 + e \cos \psi_r)^2} \\ & \times \left[(1 - e)^2(1 - \cos \psi_r) \frac{\Sigma_1 F_1}{\kappa_1} + (1 + e)^2(1 + \cos \psi_r) \frac{\Sigma_2 F_2}{\kappa_2} \right] \end{aligned}$$

- where $\chi_\theta = \chi - \chi_0$ and $\psi_r = \psi - \psi_0$. The Boyer-Lindquist and tetrad formalisms give identical results for the forced motion.

Black Hole Osculating Orbits - Schwarzschild

- In Schwarzschild, osculating element equations reduce to (Pound & Poisson 2008)

$$p' = \frac{2p^{7/2}(p-3-e^2)(p-6-2e\cos v)^{1/2}(p-3-e^2\cos^2 v)}{(p-6+2e)(p-6-2e)(1+e\cos v)^4} \delta f^\phi - \frac{2p^3 e(p-3-e^2) \sin v}{(p-6+2e)(p-6-2e)(1+e\cos v)^2} \delta f^r$$

$$e' = \frac{p^{5/2}(p-3-e^2) \{ (p-6-2e^2) [(p-6-2e\cos v)e\cos v + 2(p-3)] \cos v + e(p^2 - 10p + 12 + 4e^2) \}}{(p-6+2e)(p-6-2e)(p-6-2e\cos v)^{1/2}(1+e\cos v)^4} \delta f^\phi + \frac{p^2(p-3-e^2)(p-6-2e^2) \sin v}{(p-6+2e)(p-6-2e)(1+e\cos v)^2} \delta f^r$$

$$\psi'_0 = \frac{p^{5/2}(p-3-e^2) \{ (p-6) [(p-6-2e\cos v)e\cos v + 2(p-3)] - 4e^3 \cos v \} \sin v}{e(p-6+2e)(p-6-2e)(p-6-2e\cos v)^{1/2}(1+e\cos v)^4} \delta f^\phi - \frac{p^2(p-3-e^2) [(p-6) \cos v + 2e]}{e(p-6+2e)(p-6-2e)(1+e\cos v)^2} \delta f^r$$

- in which $v = \psi - \psi_0$. These equations are manifestly non-singular. Note division of self force into conservative and dissipative parts.

Applications

- **EMRI evolution under external perturbations** - e.g., drag force from gas in the spacetime or gravitational interaction with a distant perturbing body. Compute secular impact on orbit. Assess observability and induced parameter estimation errors.
- **Transient resonances** - model passage of EMRIs through orbital resonances (Flanagan & Hinderer 2010).
- **Improved approximate waveforms** - use osculating element approach to compute adiabatic average effects of self-force to improve kludge models. Can include conservative effects in an averaged way.
- **Compute full self-force evolution trajectories** - compute inspiral trajectories under influence of the self-force.

Application - “gas-drag”

- Illustrate application to EMRIs using a simple model of a drag-force. Take spatial part of the force to be proportional to spatial part of the velocity in the ZAMO frame.

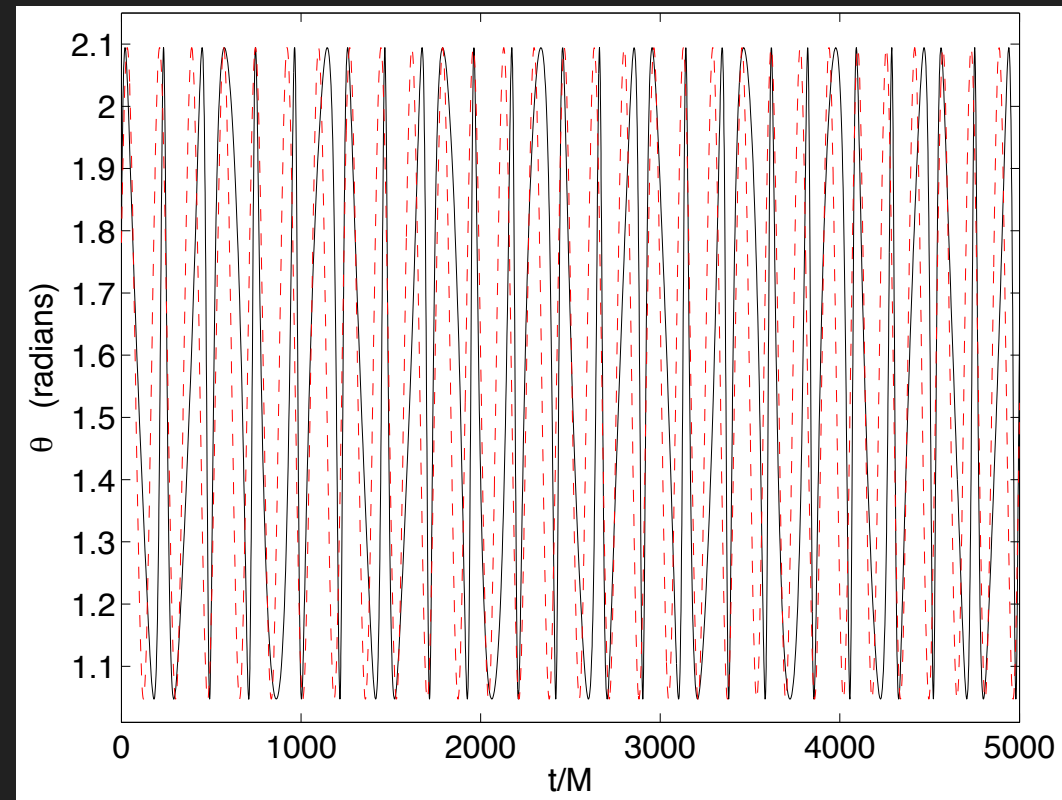
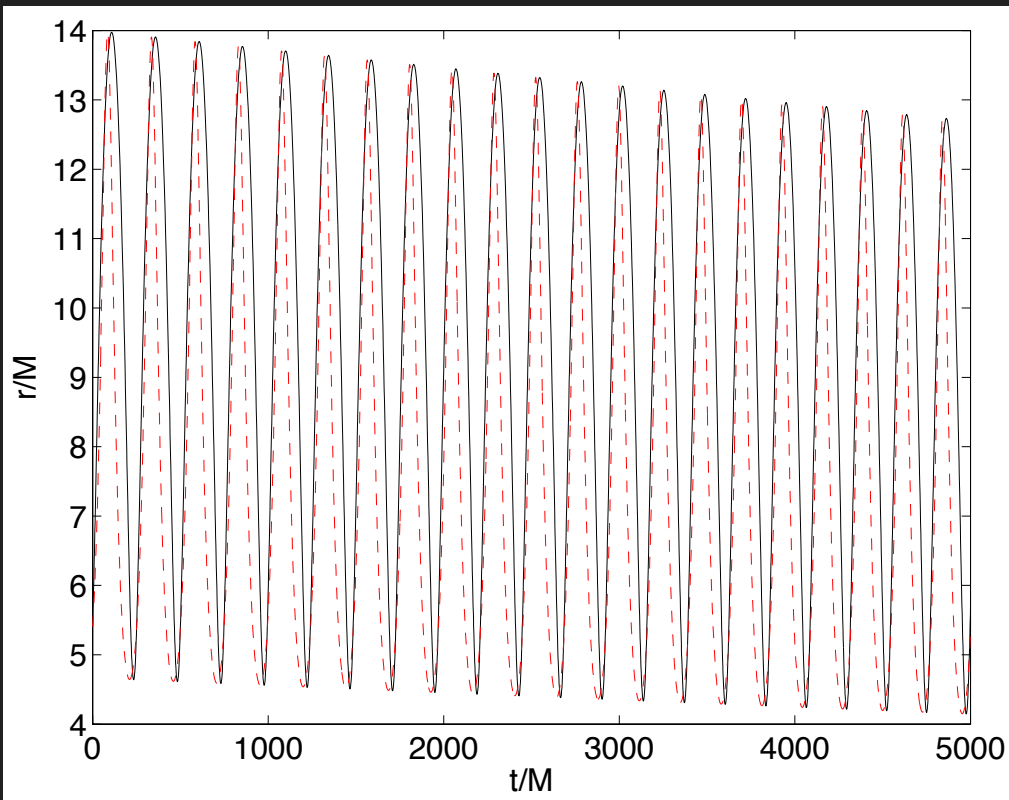
$$\vec{u}_{\perp} = \vec{u} + (\vec{u} \cdot \vec{u}_{\text{ZAMO}})\vec{u}_{\text{ZAMO}}$$

- Add piece parallel to ZAMO frame velocity in order to impose orthogonality condition

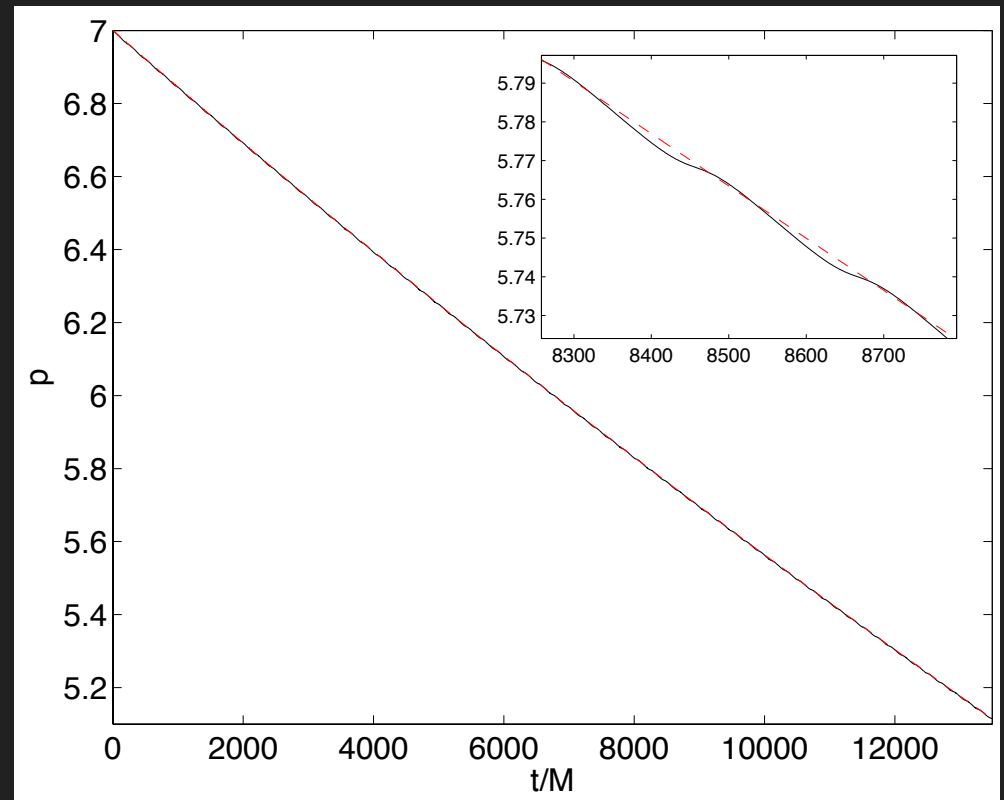
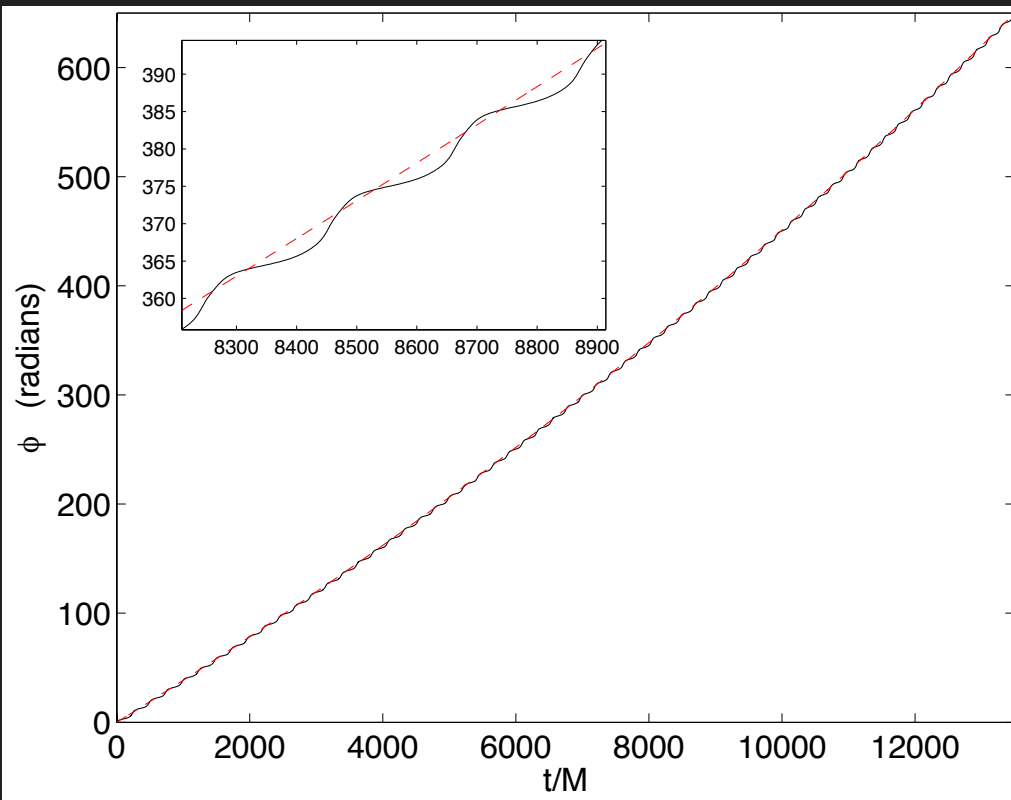
$$\delta\vec{f} = -\gamma \left(\vec{u} + \frac{\vec{u}_{\text{ZAMO}}}{\vec{u} \cdot \vec{u}_{\text{ZAMO}}} \right)$$

- Find secular decrease in semi-latus rectum and inclination, but increasing eccentricity.
- Averaged and exact evolutions show close agreement.

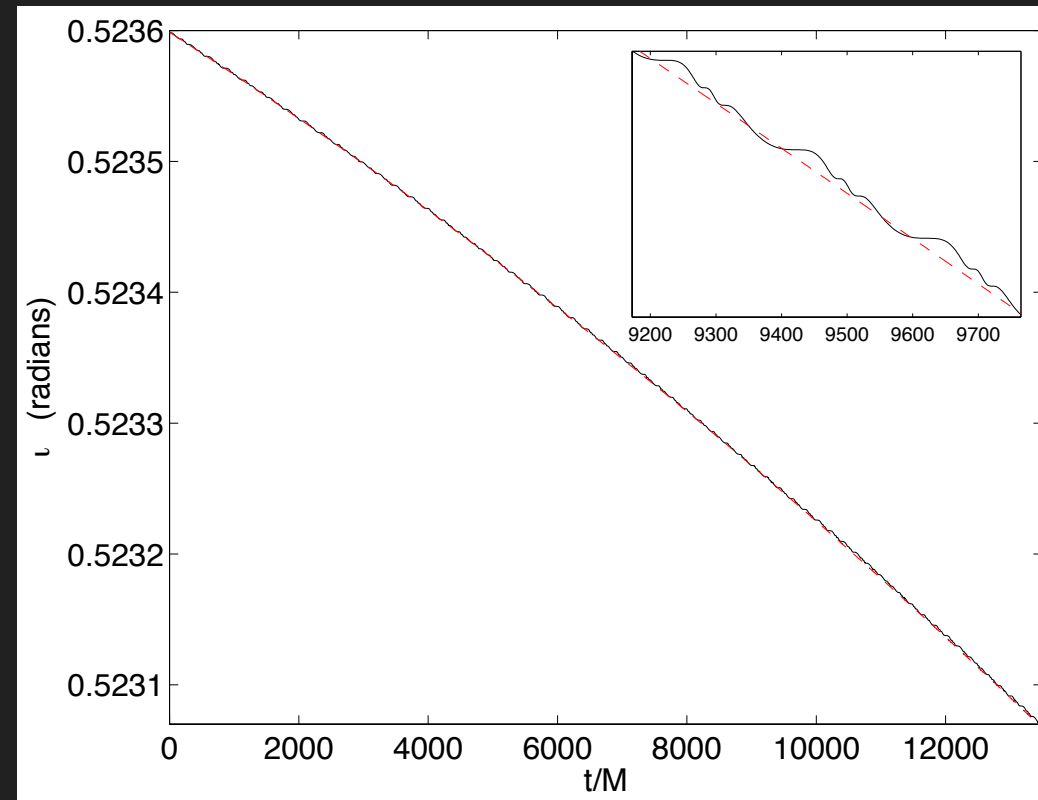
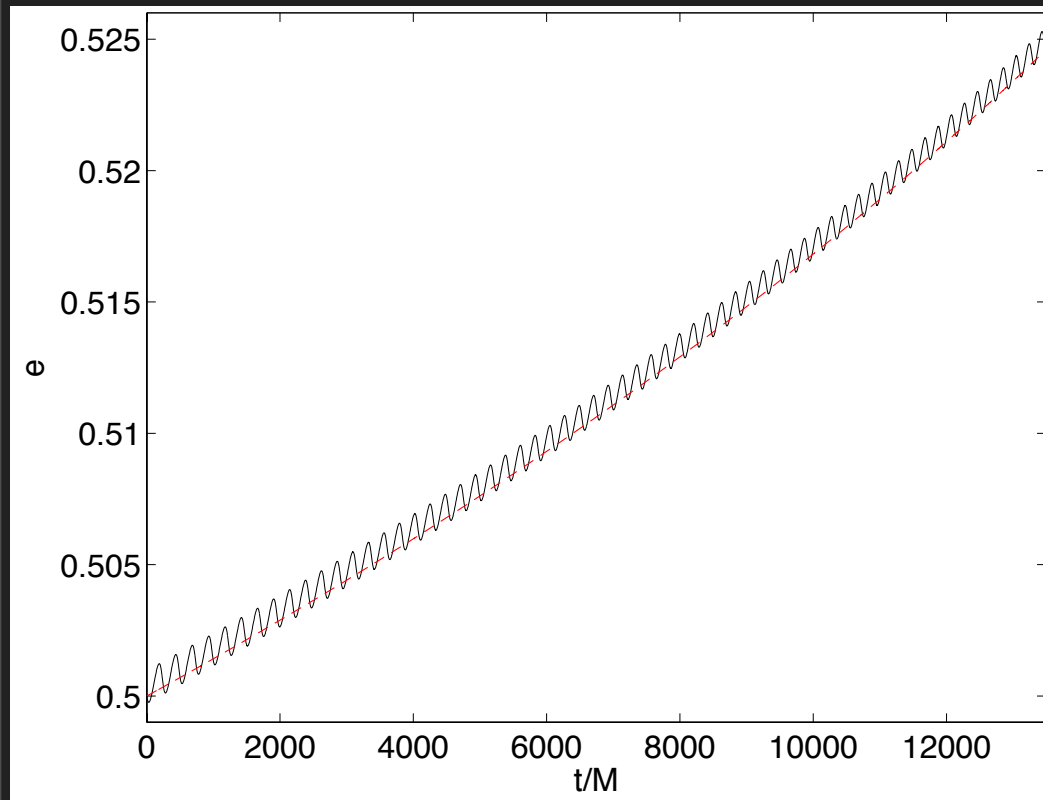
Application - “gas-drag”



Application - “gas-drag”

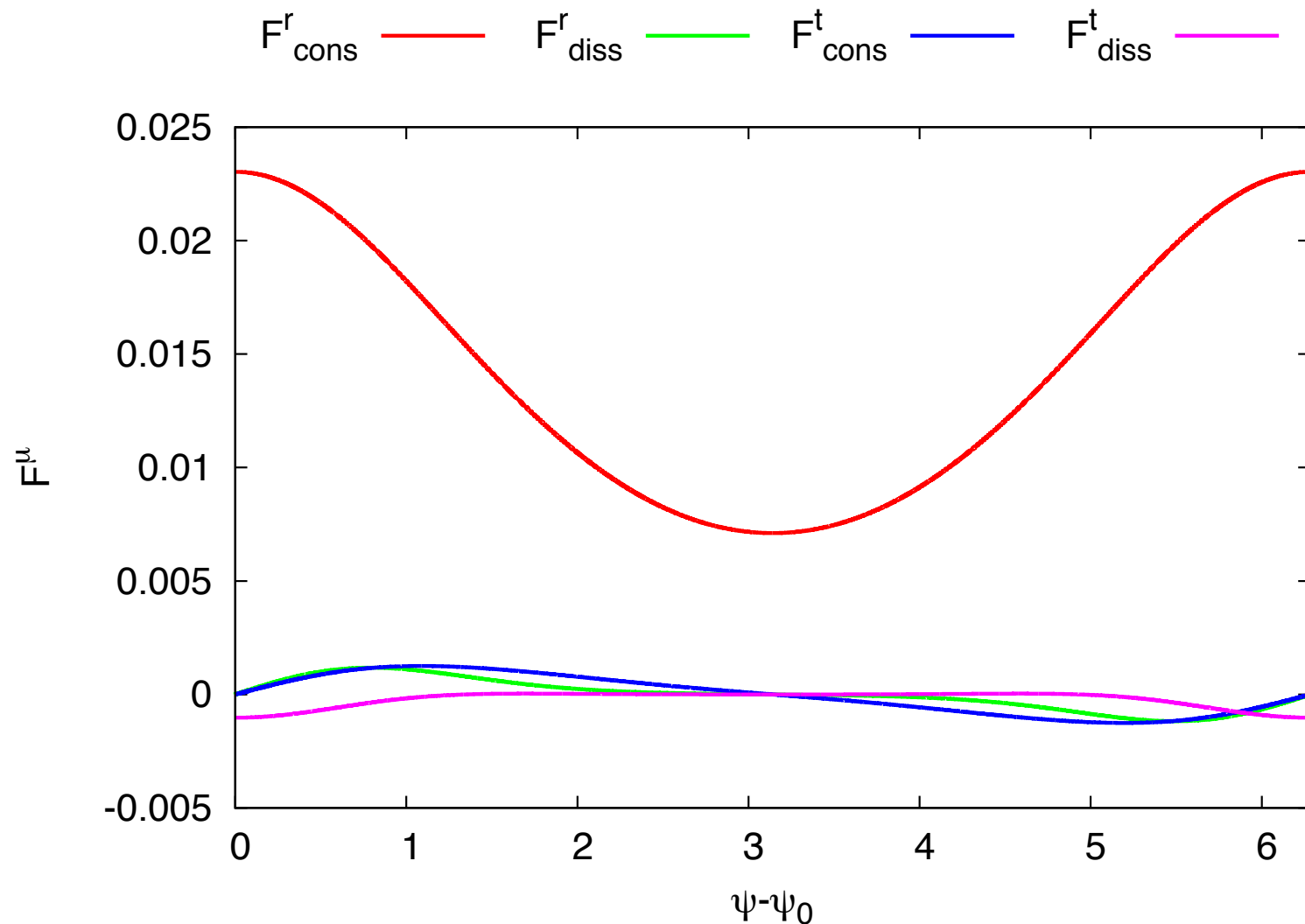


Application - “gas-drag”



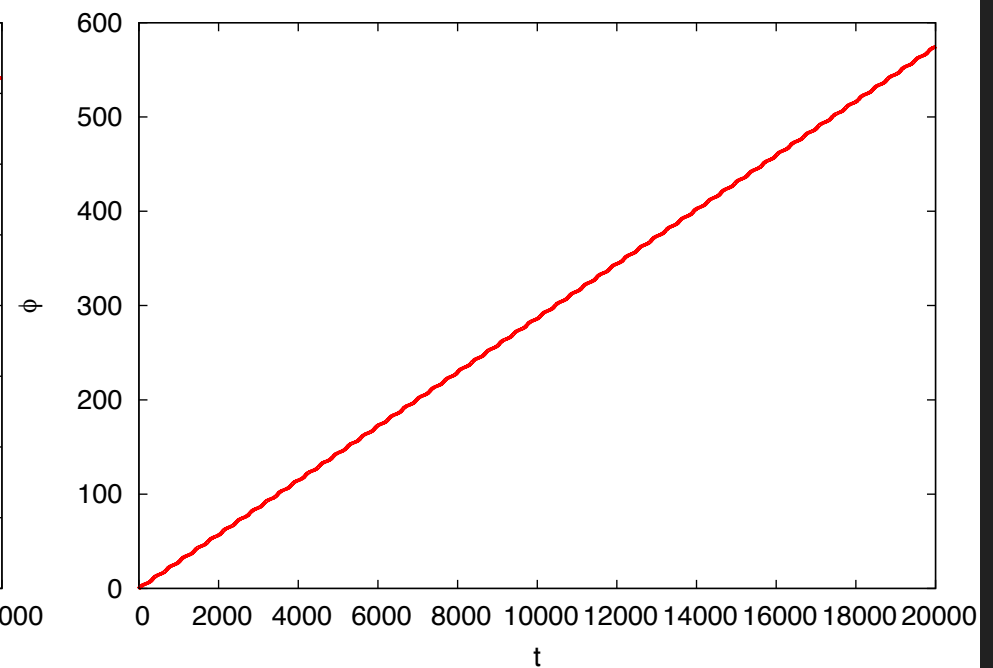
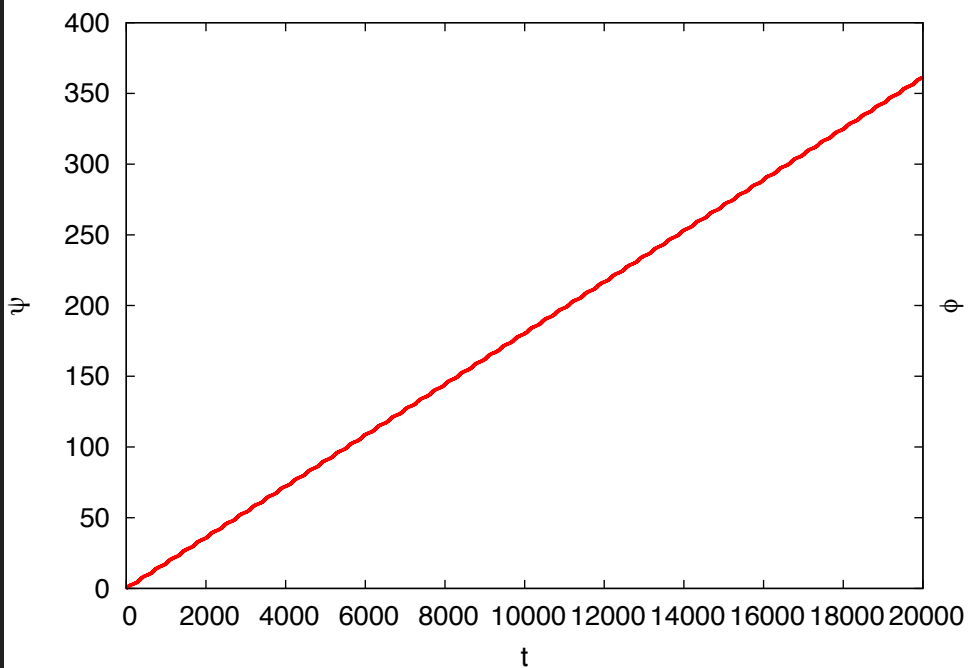
Osculating Elements and the Self-Force

- Have begun to explore self-forced evolutions using data from Warburton, Akcay, Barack and Sago.



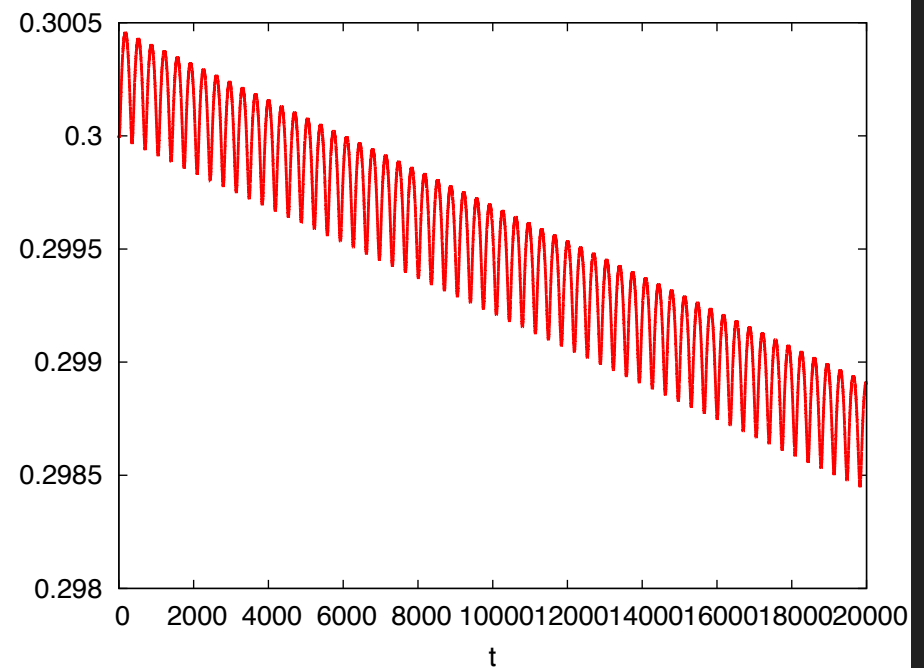
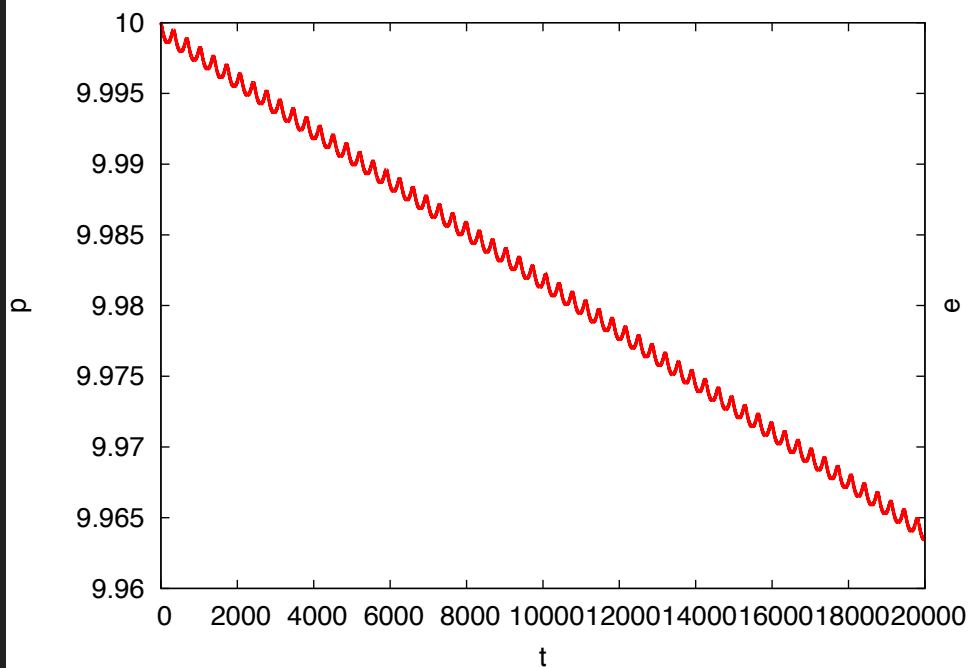
Osculating Elements and the Self-Force

- Currently have data for a handful of points, widely separated in parameter space. Explore evolution in the vicinity of these points.



Osculating Elements and the Self-Force

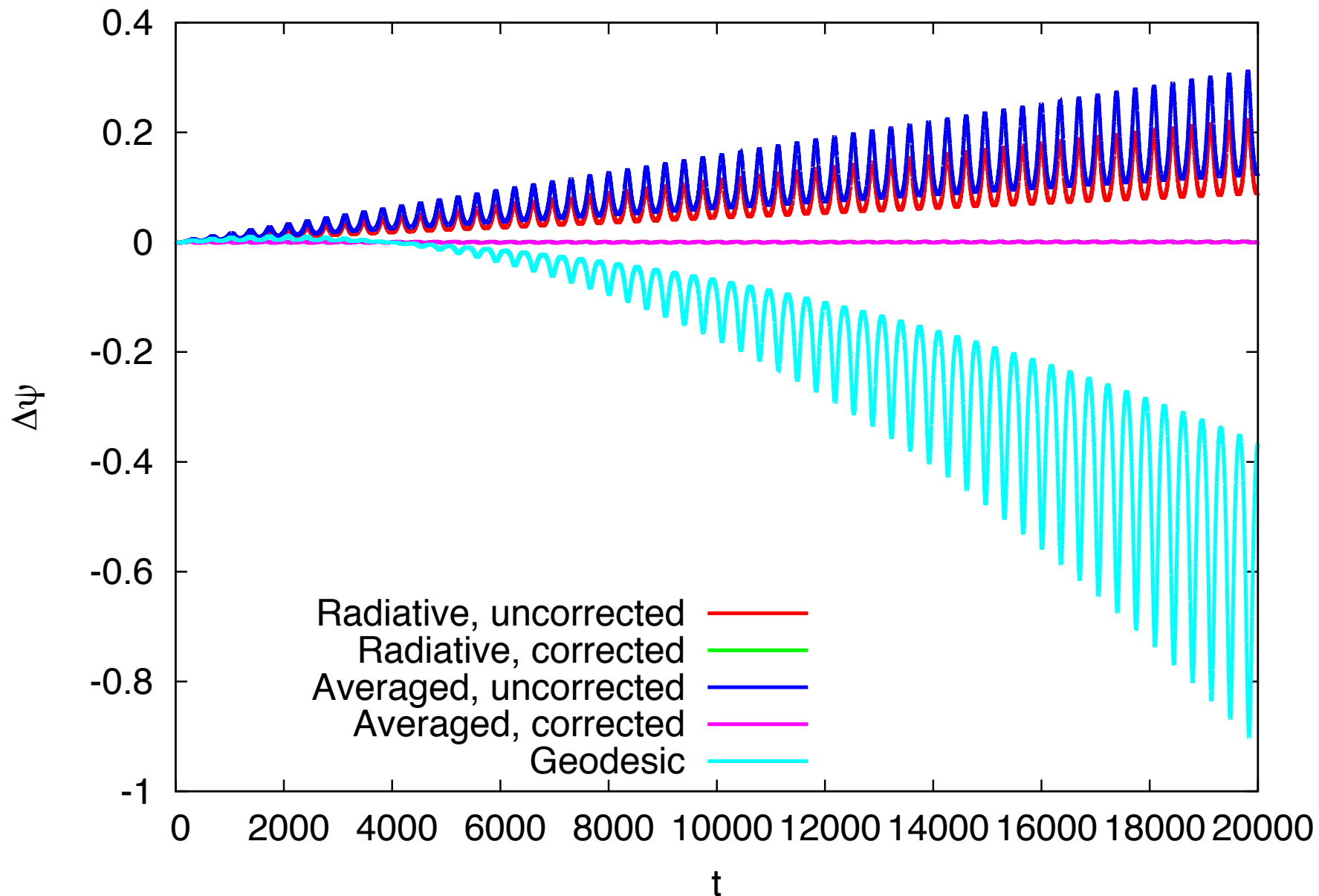
- Currently have data for a handful of points, widely separated in parameter space. Explore evolution in the vicinity of these points.



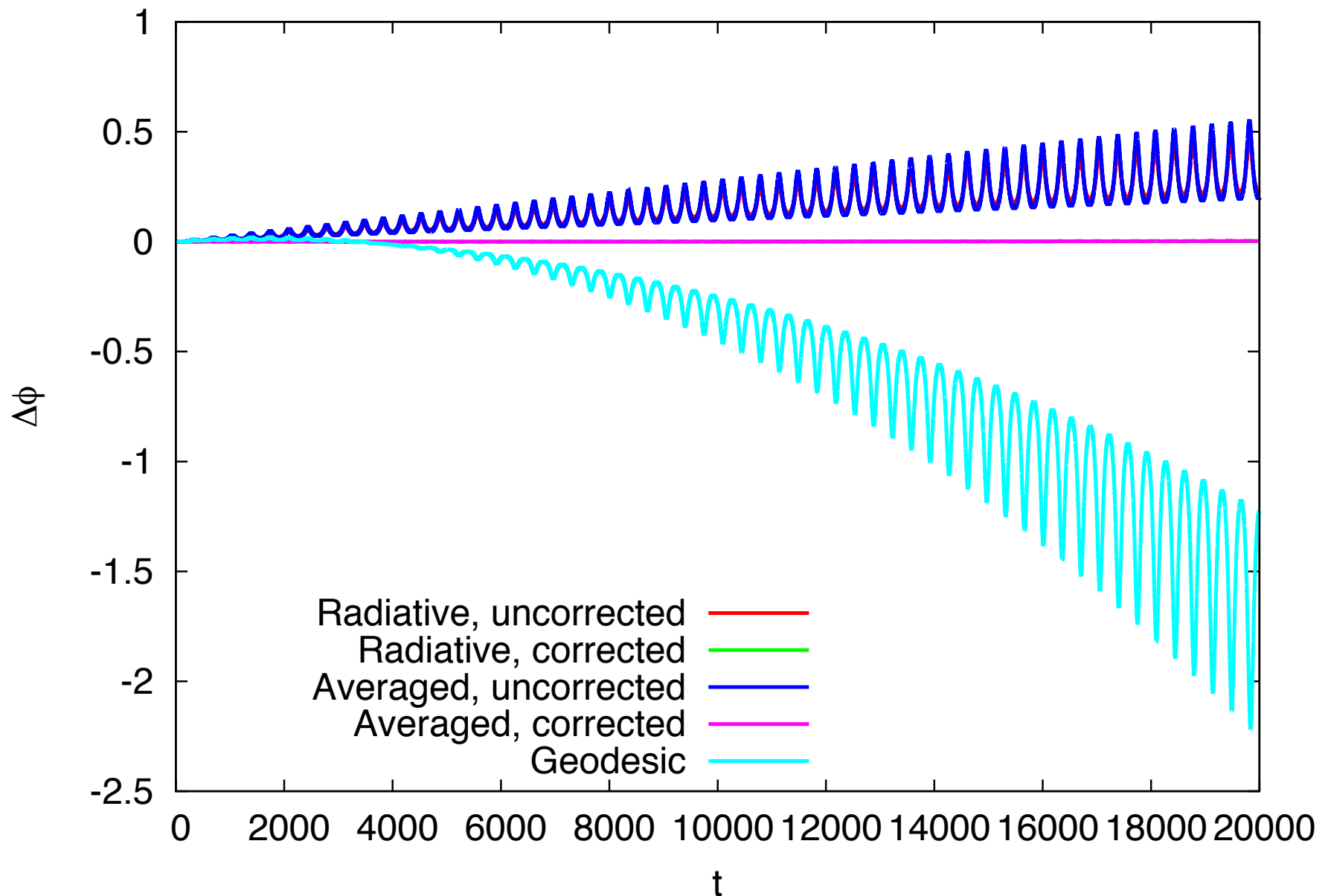
Osculating Elements and the Self-Force

- Currently have data for a handful of points, widely separated in parameter space. Explore evolution in the vicinity of these points.
- Explore various approximations
 - **Exact** - full evolution using instantaneous force.
 - **Geodesic** - geodesic motion, no evolution.
 - **Radiative, uncorrected** - evolve orbital constants, (p, e) , using orbital averaged results $\langle \dot{p} \rangle, \langle \dot{e} \rangle$.
 - **Radiative, corrected** - as above, but adjust orbital parameters to improve match.
 - **Averaged, uncorrected** - as radiative, but also add average evolution to phase offset, $\langle \dot{\psi}_0 \rangle$.
 - **Averaged, corrected** - as above, but adjust $\langle \dot{\psi}_0 \rangle, \langle \dot{\phi}_0 \rangle$ to improve match.

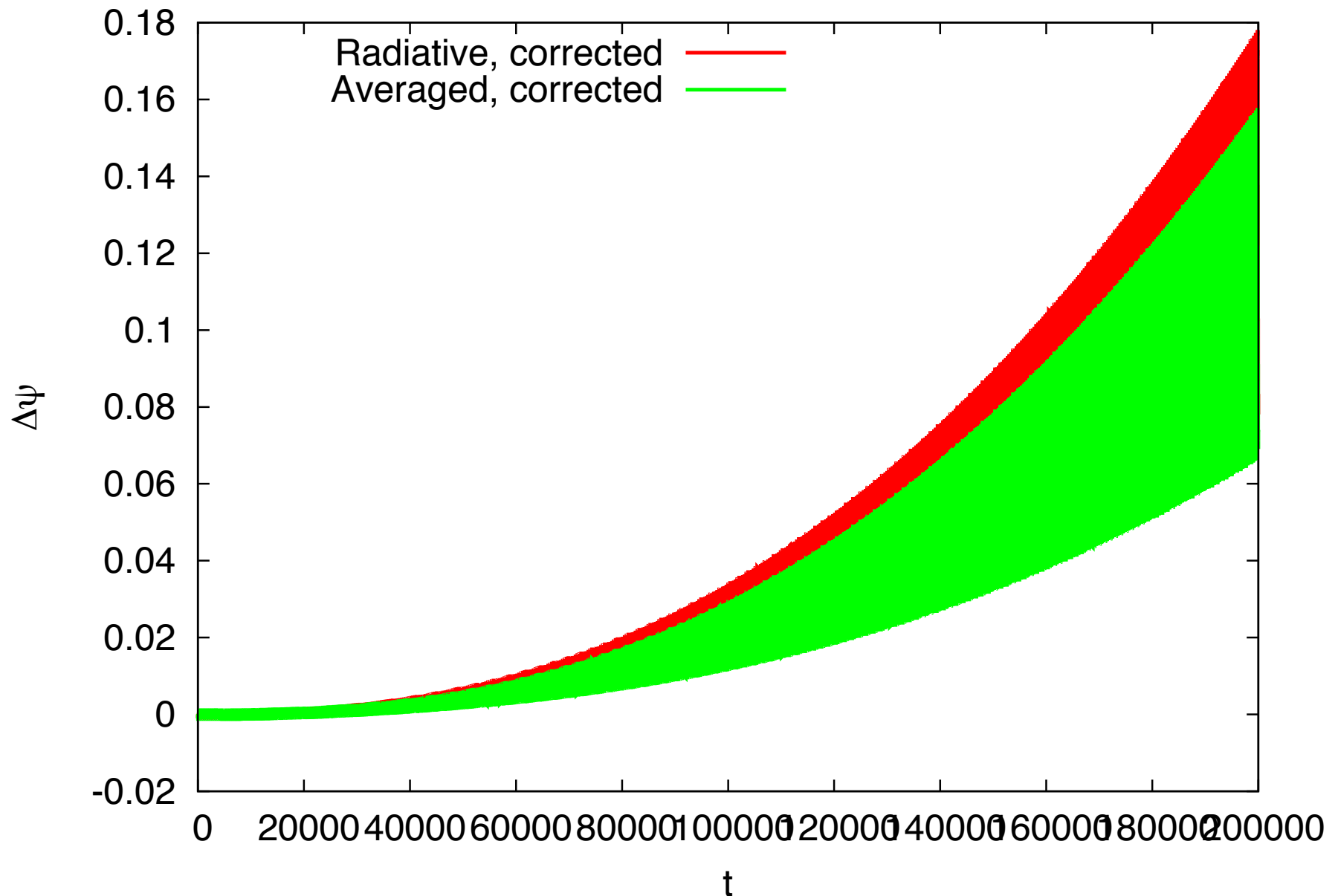
Osculating Elements and the Self-Force



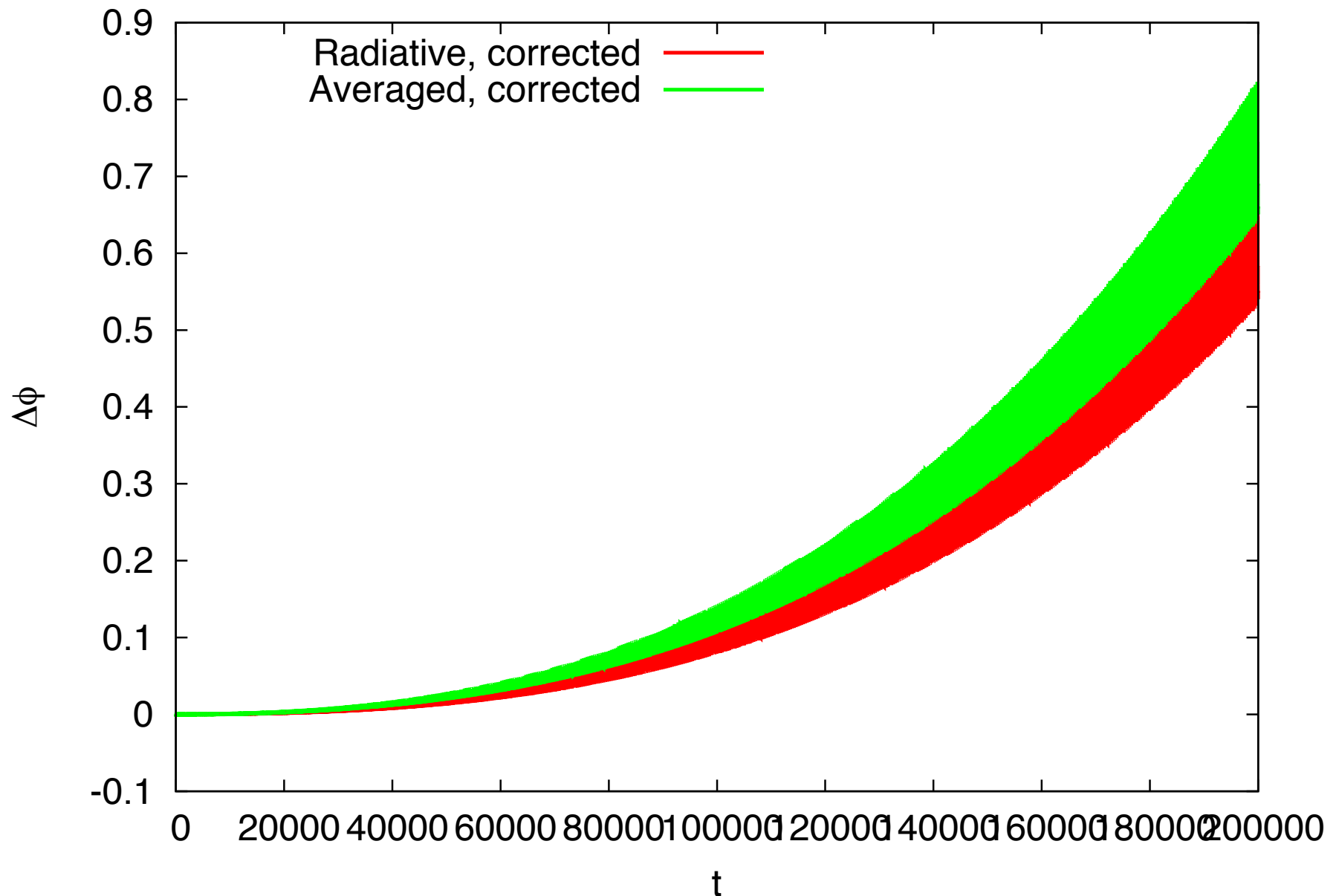
Osculating Elements and the Self-Force



Osculating Elements and the Self-Force



Osculating Elements and the Self-Force



Summary

- EMRIs are an important source of gravitational waves, but accurate modelling is difficult and computationally expensive.
- Need to be able to generate waveforms at arbitrary points in parameter space quickly and cheaply for use in scoping out data analysis, and perhaps as search templates for LISA/NGO data.
- Kludges provide a framework in which all relevant physical effects can be incorporated easily, and in a way that relates clearly to the physical system.
- Agreement with perturbative waveforms is remarkably good except for orbits very close to rapidly spinning central black holes.
- Framework for forced “osculating” evolutions has been developed. Now being used to explore EMRI perturbations.
- Have begun to explore self-forced evolutions and investigate approximations. More thorough analysis using data in wider parameter space will be coming soon....